

JGR Solid Earth

RESEARCH ARTICLE

10.1029/2020JB021171

Key Points:

- The basement of North Natal Valley and the Mozambique Coastal Plain is of continental nature
- The location of the COB is South of the Naude Ridge, close to the Ariel Graben location
- These results preclude the possibility of an overlap of the Antarctica plate on the MCP and the NNV in Gondwana kinematic reconstructions

Correspondence to:

D. Aslanian,
daniel.aslanian@ifremer.fr

Citation:

Leprêtre, A., Schnürle, P., Evain, M., Verrier, F., Moorcroft, D., de Clarens, P., et al. (2021). Deep structure of the North Natal Valley (Mozambique) using combined wide-angle and reflection seismic data. *Journal of Geophysical Research: Solid Earth*, 126, e2020JB021171. <https://doi.org/10.1029/2020JB021171>

Received 20 OCT 2020

Accepted 1 MAR 2021

Author Contributions:

Conceptualization: D. Aslanian, M. Moulin

Formal analysis: A. Leprêtre, P. Schnürle, M. Evain, F. Verrier, D. Moorcroft, S. Leroy, E. d'Acremont

Investigation: M. Evain, C. Corela, A. Afilhado, A. Loureiro, D. Aslanian, M. Moulin

Methodology: A. Leprêtre, P. Schnürle, M. Evain, P. de Clarens, J. Thompson, D. Aslanian, M. Moulin

Project Administration: M. Evain, D. Aslanian, M. Moulin

Supervision: P. Schnürle, M. Evain, D. Aslanian, M. Moulin

Visualization: A. Leprêtre, P. Schnürle, M. Evain, P. de Clarens, J. Thompson, D. Aslanian, M. Moulin

Writing – original draft: A. Leprêtre, D. Aslanian

Writing – review & editing: P. Schnürle, M. Evain, D. Aslanian, M. Moulin

© 2021. American Geophysical Union.
All Rights Reserved.

Deep Structure of the North Natal Valley (Mozambique) Using Combined Wide-Angle and Reflection Seismic Data

A. Leprêtre^{1,2}, P. Schnürle¹ , M. Evain¹ , F. Verrier¹, D. Moorcroft³, P. de Clarens⁴, C. Corela⁵, A. Afilhado⁶, A. Loureiro⁵ , S. Leroy⁷ , E. d'Acremont⁷ , J. Thompson¹, D. Aslanian¹ , and M. Moulin¹ 

¹IFREMER, REM/GM/LGS, Centre de Brest, Plouzané, France, ²LGO, IUEM, Plouzané, France, ³Nelson Mandela Metropolitan University, Port Elisabeth, South Africa, ⁴TOTAL, R&D, Pau, France, ⁵IDL – Instituto Dom Luis, Lisboa, Faculdade das Ciências da Universidade de Lisboa, Lisboa, Portugal, ⁶ISEL – Instituto Superior de Engenharia de Lisboa, Lisboa, Portugal, ⁷Sorbonne Université, CNRS, Institut des Sciences de la Terre de Paris, Paris, France

Abstract The North Natal Valley (NNV) and the Mozambique Coastal Plain (MCP) are key areas for the understanding of the SW Indian Ocean history since the Gondwana break-up. Nevertheless, the deep structures and the nature of the NNV and MCP remain discussed in the absence of deep geophysical data. In 2016, the NNV, MCP and Limpopo margin (LM) have been investigated along seven wide-angle and MCS profiles. The combined wide-angle and reflection seismic interpretation along the N-S MZ7 profile reveals an upper sedimentary sequence characterized by low velocities generally not exceeding 3 km/s, with thicknesses varying from 0.150 km in the central part to ~2.8 km in the south. The underlying sequence is formed of a 2.53.0 km thick volcano-sedimentary sequence which presents important lateral and with depth changes and presence of high velocity lenses, indicating inter-bedded volcanic sills and recurrent magmatic episodes. The south of the NNV including the Naude Ridge (NR) presents a disturbed sedimentary cover with structural highs and southward-dipping reflectors and sub-basins. The crust, reaching 35–40 km onshore below the MCP, gently thins below the continental shelf to a regular thickness of ~29 km below the NNV. Crustal velocities reveal low velocity gradients, with atypical high velocities. South the ND, the crust thins to 15 km. We interpret the velocity architecture combined with the evidences of volcanism at shallower depths as indicating an intensively intruded continental crust. Contrary to what is proposed in most geodynamic models, the Mozambique Coastal plain and the Natal Valley are both of continental nature, with an abrupt necking zone located south of NR. The Antarctica plate was therefore situated at the eastern limit of these two domains before the Gondwana breakup.

Plain Language Summary About 200 Ma ago, the mega-continent Pangaea broke up. The dispersion of the pieces of this mega-continent, linked to the closure and disappearance of the Thetys paleo-ocean, gave the birth of the Atlantic and Indian Oceans. In detail, the initial position of each piece of this jigsaw is of great importance as it has an impact on the palaeotopography and paleogeography, and our understanding of the genesis of the continental passive margins, the role of tectonic inheritance, the pre-rift and post-rift evolution of the topography dynamic (vertical movement) and of the geodynamic of the plates (horizontal movement). Nevertheless, in the Western Indian Ocean, the initial pre-beak-up position of Antarctica plate respect to Africa plate is still under debate, mainly due to the lack of deep geophysical data. In 2016, an academic-industrial collaboration succeeded in acquiring deep information along seven seismic profiles crossing the North Natal Valley off the coast of Mozambique. The results falsify the presence of an oceanic crust in that area and thus most of the plate reconstruction models. They also argue in favor a new paradigm for the genesis of continental passive margin.

1. Introduction

The North Natal Valley (NNV) forms the northern part of a N-S trending submarine basin evolving at 500–2000 m water-depth off South-East Africa (Figure 1). It is bordered to the North by the onshore Mozambique Coastal Plain (MCP) and to the South and the South-East by the offshore South Natal Valley (SNV) and Mozambique Ridge (MozR), respectively. The notable structures of the Naude Ridge (NR) and the Ariel Graben (AG) separate the NNV from the SNV and the MozR. To the West, the NNV is flanked inland by the

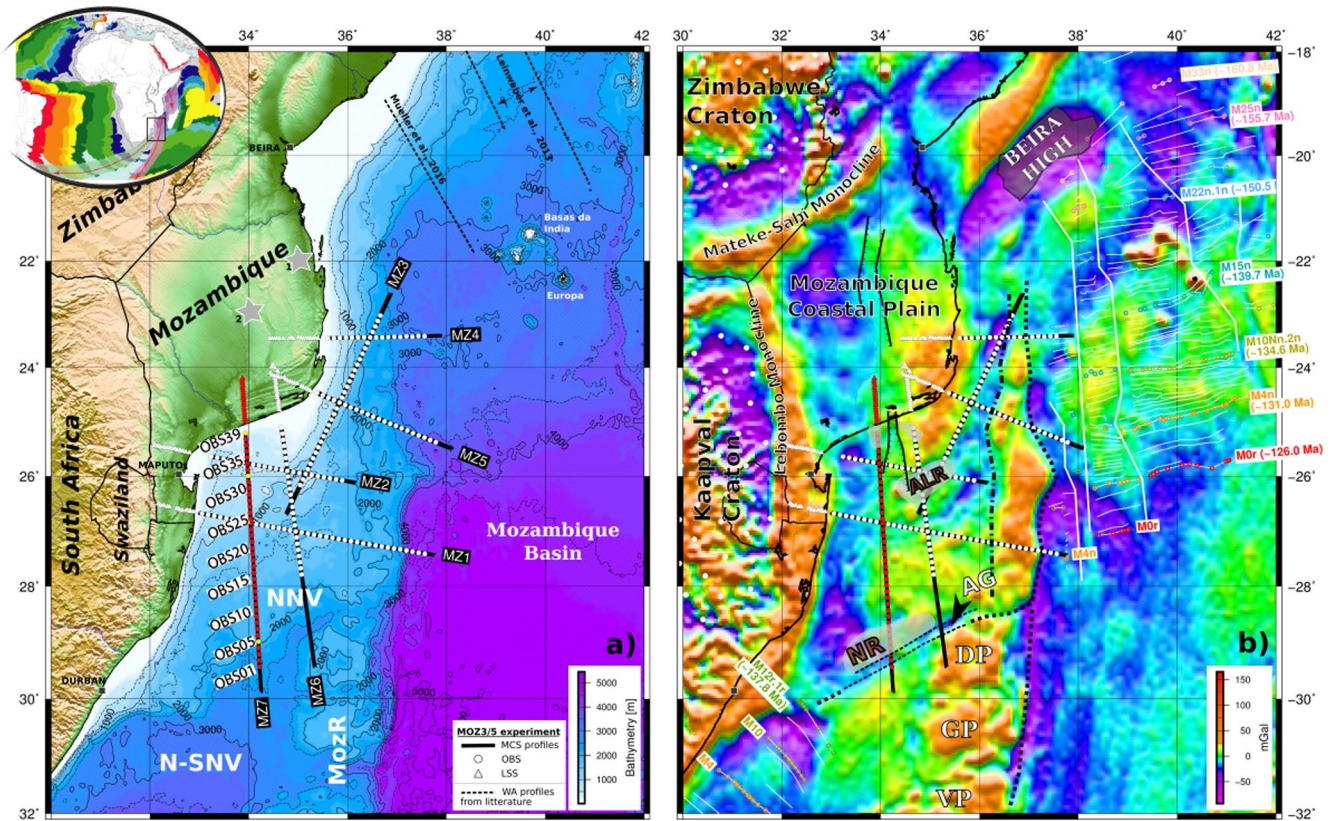


Figure 1. Location of the wide-angle seismic MZ7 profile and the MOZ3/5 experiment, SouthMozambique. (a) on topographic (GMRT grid, Ryan et al., 2009) and bathymetric (GEBCO) map. The gray stars indicated the location points of 1D Vs-depth profiles from Domingues et al., 2016. Inset: schematic cartoon that simplifies the geodynamic evolution of the area (b) on free-air gravity anomaly (Sandwell & Smith, 2009). The main features known in the area are from Mueller and Jokat (2019), which are based on Leinweber and Jokat (2012) and Mueller and Jokat (2017) for the magnetic spreading anomalies in the Mozambique Basin, and on Goodlad et al. (1982) for the magnetic anomalies in the South Natal Valley. The outline of the Naude Ridge, the South and East Tugela Ridges are from Goodlad (1986). OBS and LSS locations from the MOZ3/5 experiment are indicated by circle and triangle, respectively. Stations along the MZ7 profile are indicated in red, except those presented in the following article that are highlighted in yellow. AG, Ariel Graben; DP, Dana Plateau; E-TuR, East Tugela Ridge; GP, Galathea Plateau, Vauban Plateau; MG, Mazenga Graben; NNV, North Natal Valley; NR, Naude Ridge; SNV, South Natal Valley; S-TuR, South Tugela Ridge.

N-S oriented Lebombo Monocline and the Kaapvaal Archean Craton, while to the East, it is bounded by the Mozambique Fracture Zone before the Mozambique deep Basin.

The origin of the onshore Mozambique Coastal Plain and the offshore North Natal Valley is a key for understanding the initial Gondwana break-up stage and more particularly, the dislocation of South America, Africa and Antarctica (e.g., Cox, 1992; Goodlad et al., 1982; König & Jokat, 2010; Leinweber & Jokat, 2012; Martin & Hartnady, 1986; Mueller & Jokat, 2019; Nguyen et al., 2016; Reeves et al., 2016; Thompson et al., 2019). So far, the nature and origin of the two domains as the location of the Continent Ocean Boundary (COB) South Mozambique remain largely enigmatic and controversial in the absence of deep seismic data in the area. It results in a large variety of kinematic models for the Indian Ocean suggested over the years as summarized by Mueller and Jokat (2019) and Thompson et al. (2019), with the important question of a possible overlap of the Antarctica plate onto the Africa plate, and more precisely, on the MCP and the NNV. The overlapping of few hundred kilometres of two different continents raises questions as to the nature of the crust underlying these areas of overlap: they cannot both be of thick continental crusts (Moulin et al., 2010; Thompson et al., 2019). When tight fits imply an oceanic origin of the MCP and the NNV, looser fits suggest a continental nature (Thompson et al., 2019). Depending on the considered model, the COB is consequently located at different positions (see Thompson et al., 2019 for a review): just East and South of the Lebombo and Mateke-Sabi Monoclines respectively or slightly further inside the MCP (Klausen et al., 2009; Leinweber & Jokat, 2011; Martin & Hartnady, 1986; Mueller & Jokat, 2019), in the northern part of the NNV (Mueller & Jokat, 2019) or at the southern end of the NNV (Goodlad, 1986; Hanyu et al., 2017; Moulin et al., 2020)

(Figure 1). Additional complexities in the understanding of the Natal Valley history come from the probable interplay between the ~N-S movement between Africa and Antarctica and the ~NE-SW movement dominating between Africa and South America, and which one a model may favor. By contrast, the emplacement of oceanic crust in the SNV is well admitted thanks to better expressed NW-SE Early Cretaceous magnetic anomalies identified E-SE of Durban (Goodlad et al., 1982).

In order to provide better constraints on the origin and nature of the features South Mozambique, the North Natal Valley and the East Limpopo margins (East MCP) have been investigated during the deep seismic MOZ3/5 cruise (2016), as one part of the multidisciplinary PAMELA project (PASSive Margins Exploration Laboratories), conducted by TOTAL, IFREMER, in collaboration with Université de Bretagne Occidentale, Université Rennes 1, Université Pierre and Marie Curie, CNRS and IFPEN. The MOZ3/5 experiment was implemented to determine the crustal architecture, and more broadly to understand the evolution of this poorly-known margin at the junction of a divergent (North Natal Valley) and strike-slip (East Limpopo margin) segment, and to test kinematic hypotheses of the dislocation of the East Gondwana.

The present study focuses on the MZ7 profile, a 630 km long onshore-offshore wide-angle line, oriented in a N-S direction (Figure 1). It spans from the MCP to the N-SNV, and crosses the whole North Natal Valley, Naude Ridge and the Ariel Graben, highlighting the different segments of the ~N-S divergent margin of the Natal Valley related to the movement between the African-Antarctica-South American plates. This paper describes the multi-channel seismic (MCS) line, the ocean-bottom seismometer (OBS) and land seismic station (LSS) data, the associated traveltime forward modeling of the wide-angle profile as the coincident, and details different approaches of modeling assessment. We discuss the interpretation of the P-wave velocity model, the crustal nature and the associated implications for the MCP and NNV origin.

2. Geological & Tectonic Background

2.1. The Nature of the MCP and NNV

What is known about the crustal affinity of the MCP and the NNV is mainly based on potential field data and plate tectonic reconstructions. Green (1972) first proposes the existence of oceanic crust in the NNV using magnetic data considering the MozR as an N-S accretion center. Still mainly based on the interpretation of poorly defined SW-NE to E-W magnetic anomalies, a number of study also favor (at least partly) the oceanic origin of the NNV and the MCP (e.g., Leinweber & Jokat, 2011; Martin & Hartnady, 1986; Mueller & Jokat, 2019; Tikku et al., 2002).

Alternatively, based on vector geomagnetic anomaly, the recent study of Hanyu et al. (2017) suggest that the NNV and the North part of the MozR are floored by a mixture of stretched continental crust with basaltic intrusions. Using gravity the authors estimate a crustal thickness from 11 to 14 km in the NNV and no major change in the MCP compare to the NNV, at least in its southern and eastern part. Their values are strongly lower than the crustal thickness estimated in the MCP using ambient noise tomography from 20 to 30 km by Domingues et al. (2016) (see locations of estimation gray stars, Figure 1). Furthermore, this latest study also rules out the presence of oceanic crust on the base of the low S-waves crustal velocities characterizing the MCP. In the same way, earlier studies had already suggested the presence of thinned or transitional continental crust in the NNV and the MCP (Darracott, 1974; Dingle & Scrutton, 1974), with a total crustal thickness of the order of 25 km in the NNV from gravimetric modeling (Darracott, 1974).

Finally, the recent study of Mueller and Jokat (2019) proposes that the NNV and MozR consist of thickened oceanic crust, with an emplacement between M26r-M18n (157.1–144 Ma) and M18n-M6n (144–131.7 Ma), respectively. The emplacement of the northern part of the SNV (M18n to M15n, 144–139.6 Ma) is there also related to the N-S directed spreading between Africa and Antarctica whilst most of its southern part is connected to the separation of South America. With this hypothesis, the MCP and the NNV are emplaced in response to the ~N-S movement of the Antarctica plate, with an initial position of Antarctica overlapping the MCP and the NNV.

Finally, some models proposed a continental crustal affinity. This hypothesis prevents recovery between Africa and Antarctica in agreement with the new looser kinematic fit presented in Thompson et al. (2019). In this model, the Antarctica plate is initially located East of the NNV, with a position of the Kaapvaal Craton

(Africa) and Grunehogna Craton (Antarctica) on both sides of the NNV. The MCP and the NNV are there interpreted as part of the Africa-South American Segment, by contrast with the Africa-Antarctica segment implied by the first hypothesis. Furthermore, no horizontal movement are considered during the Kimmeridgian but the authors suggested the emplacement of mafic intrusions in the NNV at that time, whereas the oceanic spreading started North of the Mozambique Basin (M25, ~154 Ma). This episode is proposed to be responsible of the overloading of the NNV compare to the MCP (Moulin et al., 2020), and followed in the Early Cretaceous by the beginning of the Patagonia movement (South America) and the oceanisation the SNV at chron M12 or M10 (135–125 Ma) as proposed by Goodlad et al. (1982).

2.2. Nature and Origin of the Ariel Graben and Naude Ridge

Located at the southern boundary of the NNV, the Ariel Graben (AG) is SW-NE oriented structure characterized by pronounced negative magnetic (Hanyu et al., 2017) and gravity anomalies (Figure 1), whilst the Naude Ridge (NR), following the same orientation, corresponds to morphological highs generally correlate with a strong positive magnetic anomaly. Both structure separated the NNV from the SNV and their different magnetic patterns (Hanyu et al., 2017; Mueller & Jokat, 2019). The origin of the AR, as the NR, remains unclear and is closely related to the prior consideration of the crustal nature of the NNV as the kinematics models.

In their recent study, Mueller and Jokat (2019) proposed that the signature of the AG might be due to an edge effect there induced by the presence of a thinner crust in the SNV as a possible increased in magmatism during the separation with the South American plate, while considering an oceanic nature in both North and South Natal Valley. Additionally, the authors suggested the possible overprinted of original magnetic signature by more recent intruded magmatism in this zone of weakness. Considering an over-thickened oceanic crust in the NNV, Mueller and Jokat (2019) inferred that the AG marked an area of ridge jump around M18n (~144 Ma) from the NNV to the N-SNV. This interpretation therefore excludes an eventual link between the position of the COB and the structures of the NR and the AG. Mueller and Jokat (2019) proposed a scenario with the COB situated far North, in the MCP.

By contrast, Hanyu et al. (2017) consider a NW-SE oriented stretching linked to the rifting between South America and Antarctica in the northern part of the SNV, and the subsequent rotation of the Dana and Galatheas Plateaus (GP) part of the Mozambique Ridge (Figure 1) that leads to the formation of the AG (146–130 Ma). The authors suppose there a continental crustal affinity of the NNV as well as in the N-SNV including basaltic intrusions. According to their interpretation, a first phase of extensional faulting occurred in the continental NNV and North MozR during the initial break-up after ~183 Ma, and subsequently Karoo volcanism (e.g., Jourdan et al., 2008) was intruded along these faults. This led them to adopt a position of the COB close to the location of the M10 magnetic anomaly in the S-SNV, just South of South Tugela Ridge (S-TuR), in agreement with the interpretation of Goodlad et al., (1982) West of longitude ~33°, and approximately following the position of the 3000 m isobath (Figure 1a) south of the MZ7 wide-angle profile and passing south of the GP to the East.

Alternatively, the earliest study of Goodlad (1986), based on seismic data as well as geological and geophysical evidences, favors a relative position of the COB also South of the S-TuR, but suggests that the NR and the East-TuR (Figure 1) may approximately be the northern extent of the oceanic crust in the Natal Valley south of the NNV, and thus close to the location of the AR. Furthermore, the study is additionally argued by the geochemicaly and petrologically analysis of basalt samples from the dredge site 5749, located in the northern part of the E-TuR, which would suggest according the author a transitional origin but with continental affinities.

3. Data Acquisition & Processing

3.1. The MOZ3/5 Experiment

The MOZ3/5 experiment was conducted onboard the *R/V Pourquoi pas?* from February 11th to April 4th 2016, seven coincident Ocean Bottom Seismometers (OBS) wide-angle seismic and MCS reflection (720 traces) profiles were collected, as well as additional data of gravimetry, magnetism, bathymetry, coring,

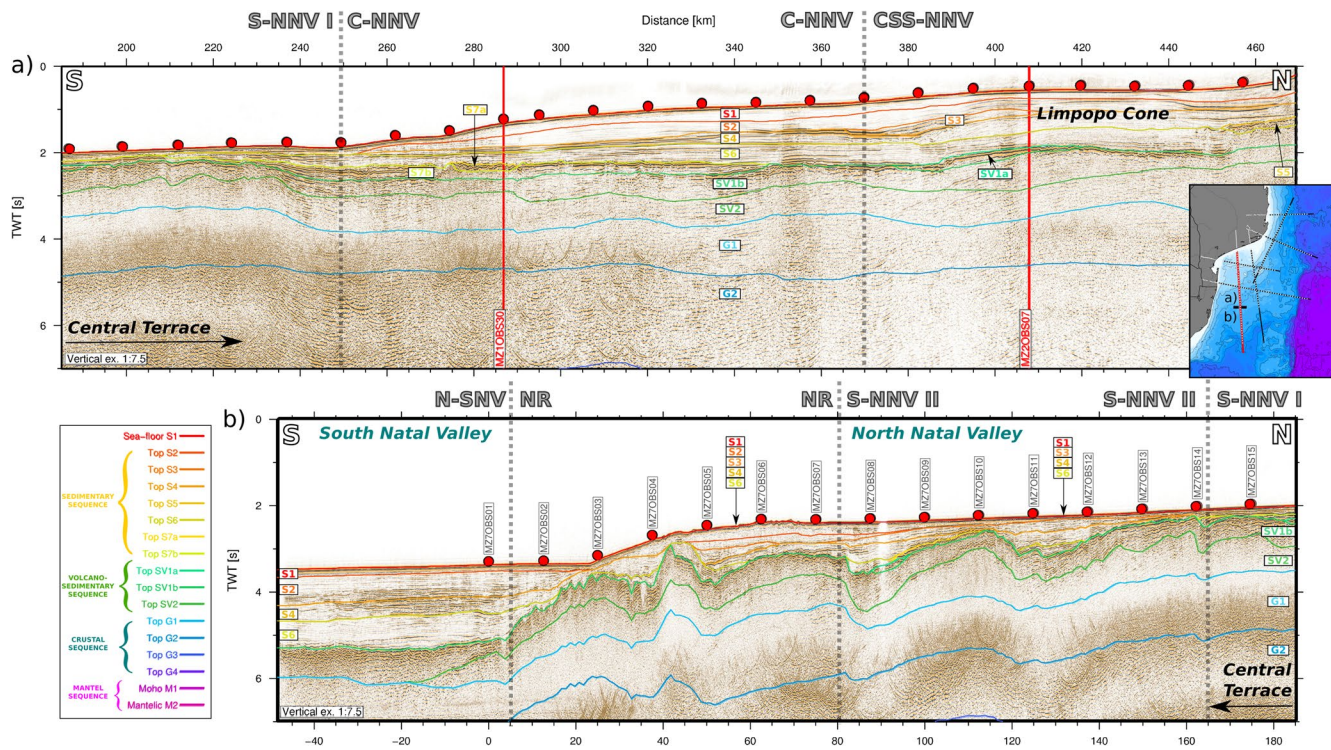


Figure 2. Two-way travel-time record section of MCS data along MZ7 profile overlain by time converted color-coded interfaces of wide-angle model. The intersections with the MOZ3/5 dataset are indicated by red line. OBS locations are indicated by red circle. Vertical exaggeration is 1:7.5.

dredging, sub-bottom and water column (Moulin & Aslanian, 2016; Moulin & Evain, 2016). Simultaneously, land seismometers were deployed in the MCP, extending six of those profiles on land for about 100 km in order to provide information on the onshore-offshore transition (Figure 1). The seismic source was composed of 15 airguns providing a total volume of 6500-in³, with a shot interval set at 60 s. In total, 3454 air-gun shots were generated along MZ7 presented here and recorded jointly by Ocean Bottom Seismometers (OBS), Land Seismic Stations (LSS) and a marine 720-channel streamer 4.5 km in length. A total of 39 OBSs (three-component geophone and an hydrophone) from Ifremer pool (Auffret et al., 2004) spaced every ~12.5 km were deployed along the 520 km long offshore part of the MZ7 profile, at water depths of 140–2540 m. The profile was extended inland with 19 LSS (Reftek 125A-01 and L-4C) spaced every 5 km and located at altitudes of 24–90 m, resulting in a landward extension of the line on about 110 km.

3.2. MCS Data Processing

The acquisition of the MZ7 profile was discontinued on three occasions due to marine mammal observations in the exclusion zone, resulting in a partitioned acquisition into four separated profile portions. On each occasion that acquisition was suspended, the vessel was required to perform a loop in order to realign the towed streamer onto the intended profile orientation, so that continuous, linear coverage of the profile could be achieved. The shots fired during the loops were then suppressed to ensure continuity in the offset of the seismic traces. Finally, initial and final shot recordings of each profile portion were identified, allowing for accurate and continuous merging of shot records from the four separate profile portions, without the risk of overlapping or discontinuous coverage. Vertical bands of altered signal are nevertheless visible at the junction between each portion at km ~90, 350, 400 (Figure 2).

A first quality control and pre-processing was undertaken on the reflection seismic data using the *SISPEED* software (Ifremer), and further processing of the MCS data was then performed using the *GEOCLUSTER* software (CGG Veritas). The processing sequence was composed of geometry, wide butterworth frequency filter (2-12-64-92 Hz), resample traces from 2 to 4 ms, spherical divergence compensation, deconvolution, Common Mid Point (CMP) sorting, water-bottom multiple attenuation, frequency filter (2-12-48-64 Hz),

surface-related multiple modeling and attenuation, editing and water column mute, velocity analysis, Kirchhoff pre-stack time migration, update of the velocity analysis, normal move-out correction, multiple attenuation in the radon domain, dip move-out, CMP stacking, F-k migration and, Kirchhoff post-stack time migration.

3.3. Wide-Angle Data Processing

Pre-processing of the OBS data included internal clock-drift correction to the GPS base time, and correction of the instrument locations for drift from deployment position during their descent to the seafloor using the direct water wave. Then upward and downward traveling waves were separated (e.g., Schneider & Backus, 1964) by combining hydrophone and vertical seismometer OBS components. A spiking predictive deconvolution was applied to the upward traveling record using the downward traveling wave as signature. Spherical divergence was applied to compensate amplitude decay of the records. Traces were further scaled with a gain proportional to the offset in order to enhance the refracted events.

The data from LSSs composing an array were first debiased and band-pass filtered. The array was then stacked. In addition, the LSS data were reduced by an 8.0 or 8.5 km/s velocity which flatten the principal Pn arrivals, then processed with an FX deconvolution (in a moving $1.9 \text{ s} \times 21$ traces window) to attenuate random noise.

4. Data Analysis

4.1. Reflection Seismic Data

The quality of MCS MZ7 data is generally good, even if seismic signal does not image beyond 2.5–3 s twt below the seafloor due to the presence of numerous multiples from the seafloor and other major interfaces in the stratification, as well as probable high velocities layers (such as carbonate and/or volcanic layers) (Figure 2). From the continental shelf to the N-SNV, a very pronounced, high amplitude, low frequency reflector is identified along the whole profile, particularly clearly traceable across the southern half of the MZ7 profile. It generally corresponds to the top of the sequence labeled SV, and is further identified on all profiles acquired in the North Natal Valley during the MOZ3/5 cruise (Moulin et al., 2020).

The center of the MZ7 MCS profile is dominated by the Central Terrace (165–240 km model-distance). The area is typically characterized by a flat bathymetry, a reduce thickness of the well-bedded sedimentary layers, and a position of the highly reflective top of the SV sequence close to the seafloor (Figure 2). Indeed, this flat bathymetric plateau lies above a relative structural high on which the recent sedimentary layers come to thin and or pinch-out, from North and South.

The sedimentary “S” layers show transparent to well-bedded seismic facies with important lateral changes, as well as clear pinch-outs and discordances, sometimes indicated by strong reflectors. In this way, the contact generally of high amplitude and/or in unconformity between S2/S3–S4, S4–S6 and S6–S7 seems to indicate major events. Locally through the sedimentary sequence, reflectors appear with a rougher, rather high amplitude, and discontinuous facies, generally associated with a loss of seismic signal below at the position of the lens S5 or S7a especially (Figure 2, respectively at 450–470 km and at 270–290 km model-distance). Finally, the whole sedimentary thickness decreases southward through the Limpopo Cone along the continental shelf.

South of the Central Terrace, the southern part of the NNV, including the Naude Ridge, present a succession of southward-dipping asymmetric sub-basins and relative morphological highs (Figure 2). The sedimentary cover presents transparent to well-bedded facies, at least particularly through the lower half of the sequence, which also exhibits increasing amplitudes with depth. Reflectors are there much more disturbed than to the North, generally showing southward-dips, sometimes faulted, or even locally totally tilted toward the North and pierced by a more chaotic body (Figure 2, at 40–50 km model-distance) in the Naude Ridge area. Both observations suggest important tectonic deformation and magmatic activity, including a clearly more recent post-sedimentary activity recorded in the southern end of the NNV.

Located at the base of the upper sedimentary cover, the prominent reflector at the top of SV1a/b, as at least the SV1b layer, evolve along the line with many changes in their seismic characters, from rough to smooth, sometimes chopped or shifted, and with more or less amplitude (Figure 2). Below the strong reflector, the penetration of the seismic signal is limited although reflectors can be observed, generally more expressed through the SV1b layer and at its base, although reflectors are still discernible in some places throughout SV2. In the northern part of the profile, characterized by shallower water depths, reflectors under the Top of SV are difficult to discern due to the presence of multiples. Particularly well-bedded deep reflectors are imaged with a northward-dip directly North of the Central Terrace, between 240–250 km model-distance, and with lower amplitude South of the Central Terrace showing there an apparent opposite dip toward the South, especially through SV2 (120–160 km model-distance). By contrast, at Central Terrace the trend of the SV internal reflectors seems rather parallel to the seafloor, sometimes with a more chaotic or blanking facies, suggesting magmatic intrusions (e.g., between MZ7OBS18 and 20, Figure 2a). South of the kilometer ~120, the SV seismic facies tends to become more chaotic, suggesting a more volcanic character. The continuity further South of the geological unit including the apparent “southward-dip” reflectors directly South of the Central Terrace is unclear due to imagery limitation. It is important to note that the layers, particularly in the case of the SV sequence, are modeling layers related to the need for velocity modeling and coherence, and may sometimes not correspond to a continuous geological unit. Higher amplitude deep reflectors are locally imaged, as around the kilometer 75, there without revealing a particular dip. South of the chaotic/transparent post-sedimentary volcanic body mentioned just above, the SV1b layer internal reflectors as well as its top appear now clearly delayed at some places, suggesting the succession of a set of short wavelength faults. When arriving in the N-SNV (south of ~5 km model-distance), the top of SV becomes more regular and flat, while the seismic facies through the SV1b changes from rather well bedded with a southward inclination to more transparent and rougher South of ~ -30 km model-distance. In this area, the SV modeling layer seems to take on a completely different geological significance from that of the Natal Valley.

4.2. Wide-Angle Seismic Data & Phases Identification

The quality of the OBS records is generally very good, with arrivals up to 180–220 km offset on most instruments. Seismic records from OBSs located North of the profile on the continental shelf nevertheless appear noisier on the vertical geophone channel (Figure 3). Due to a technical problem that caused early rise of the instrument to the surface, the MZ7OBS29 did not record all the air gun shots. However, it did well record all the shots from the South and some from the North. Inland, almost all the LSS array recorded good quality data, with clear crustal and upper mantle arrivals up to 500 km offset on the northernmost LSS records. The MZ7LSS10 and MZ7LSS11 records show few seismic arrivals and MZ7LSS04 and MZ7LSS08 instruments gave no data at all. Examples of the recorded wide-angle data and ray tracing for MZ7OBS 39, 32, 30 and 05 are shown in Figures 3–5, and for MZ7LSS03 in Figure 6.

The OBS sections show low velocity sedimentary arrivals (from orange to yellow, Ps1 to Ps7b phases), except on the instrument records located along the Central Terrace where the upper sedimentary cover significantly thins on MCS (Figure 2). When observed, sedimentary arrivals are characterized by apparent velocities generally not exceeding 3.0 km/s. Before unequivocal crustal phases (Figure 5), the OBS records show arrivals characterized by intermediary apparent velocities, typically in the range 4.0–5.5 km/s, and corresponding to the volcano-sedimentary sequence (in green, SV1–SV2 phases). Generally extending over more than 200 km, clear Pg arrivals are identified on OBSs and LSSs (in blue to purple, Pg1–Pg4 phases), traveling through the crust with average apparent velocities around 7.0 km/s. By contrast, deeper arrivals from the upper mantle (in magenta, Pn phases) with apparent velocities around 8 km/s are poorly observed on the OBSs, except at the southern extremity of the line where the thinning of the crust is suggested by the PmP and Pn arrivals at shorter offsets (Figure 6). The MZ7OBS32 is one of the rare OBSs that shows identifiable Pn arrivals North of the wide-angle profile (Figure 4), probably due to an important thickness of the crust combined with the decrease in amplitude of the seismic signal with increasing offsets. Nevertheless, Pn arrivals are more recorded from the North by the LSSs, and more precisely the northernmost stations. Sedimentary reflections (PsP phases) are better observed to the North along the continental shelf, following the clear high amplitude reflectors and discontinuities on MCS. The top of the SV sequence is generally associated with the main high amplitude reflection inside the water cone, and the last having zero-offset arrival times coherent with the highly reflective, uppermost green SV1a/b interfaces interpreted

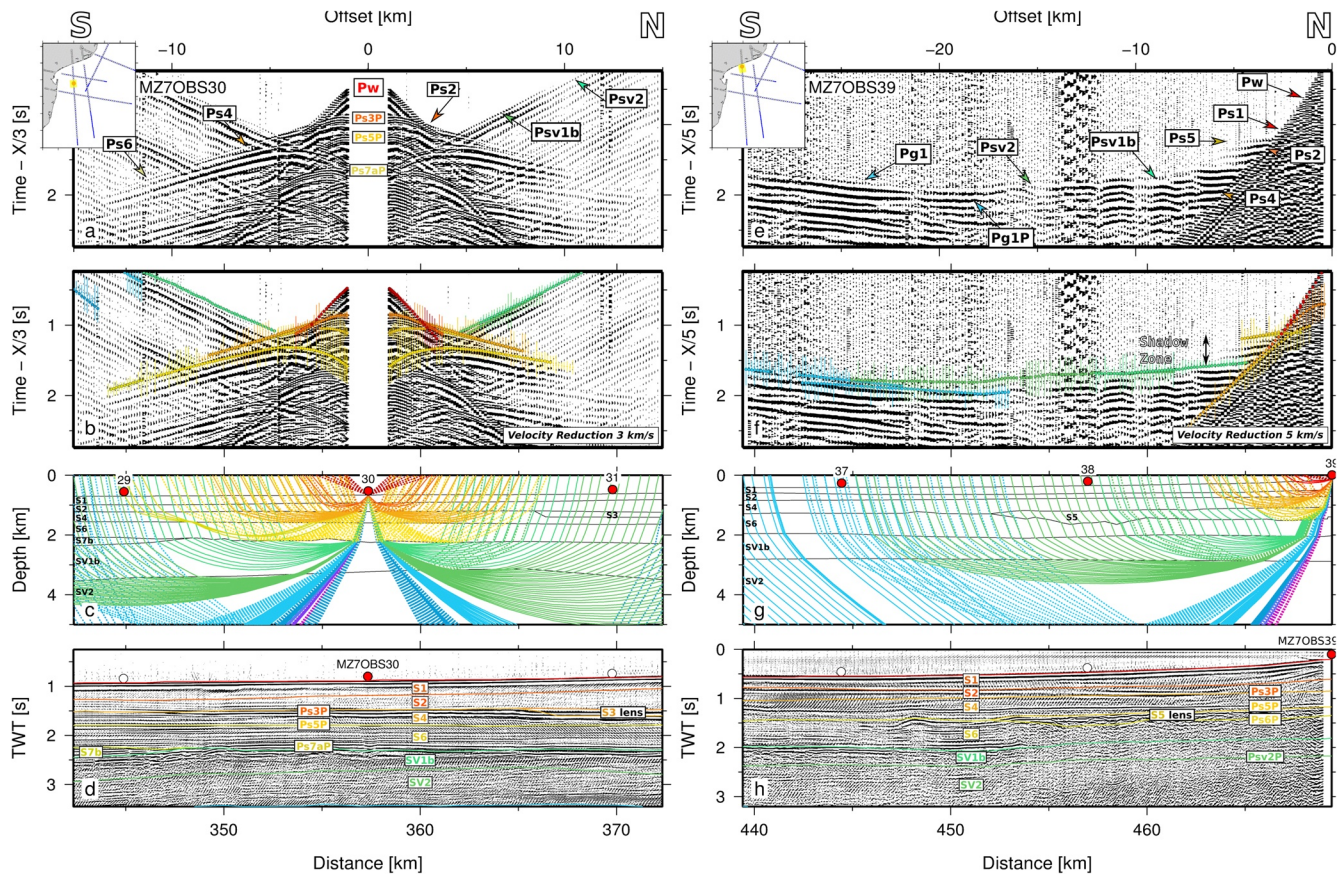


Figure 3. Data from MZ7OBS30 (left) and MZ7OBS39 (right) on MZ7 profile. (a) and (e) Vertical geophone component of the recorded section with labels of the color-coded interpreted phases. A band-pass filter (4-6-32-48), 3 km/s (left) and 5 km/s (right) velocities reduction, and an offset-dependent gain are applied. (b) and (f) Vertical geophone component of the recorded section with the color-coded observed travel-times picks (vertical bars, the size showing the uncertainty range), overlain by predicted travel-times in the final model (color-coded dots). (c) and (g) Model section showing corresponding ray-tracing. (d) and (h) MCS data with the modeling color-coded interfaces and the corresponding labeled layers and phases.

in the MCS data. Probably due to the intermediate velocities characterizing the SV sequence, the top of the crust does not generate a major reflection on OBSs or LSSs. By contrast, numerous intra-crustal reflections (PgP2–PgP4 phases) indicate a strong internal reflectivity of the crust along the North Natal Valley. Moho reflections (PmP phase) are rather well identified along MZ7, and appears locally as the top of a package of high amplitude arrivals, suggesting local internal reflectivity at proximity of the Moho and at least in the uppermost mantle.

4.3. Modeling Approach

The data were modeled using an iterative procedure of two-dimensional forward ray-tracing from the RAY-INVR software (Zelt & Smith, 1992). Modeling was performed using a layer-stripping strategy, proceeding from top (seafloor) to bottom (Moho). The velocity model is constructed layer after layer and composed of velocity and interface-depth nodes. Depth and velocities were adjusted such as to minimize the difference between the observed arrival times and the arrival times computed in the model. The seafloor bathymetry was taken from the multibeam data acquired during the MO3/5 cruise. On land, topography was included from the GEBCO data. Arrival times of the main sedimentary interfaces were picked from the coincident MCS line and integrated in the modeling, as long as they are correlated with identified phases in the OBS data to avoid over-parameterization of the model. An iterative procedure of velocity and depth adjustment, with check of the depth-twt conversion against MCS data was then applied. Such procedure is applied to all sedimentary layers up to the acoustic basement on the MCS. Beyond, we used only the arrival times from the OBS and LSS data set. Lateral topographic or velocity changes were inserted only where required by the data.

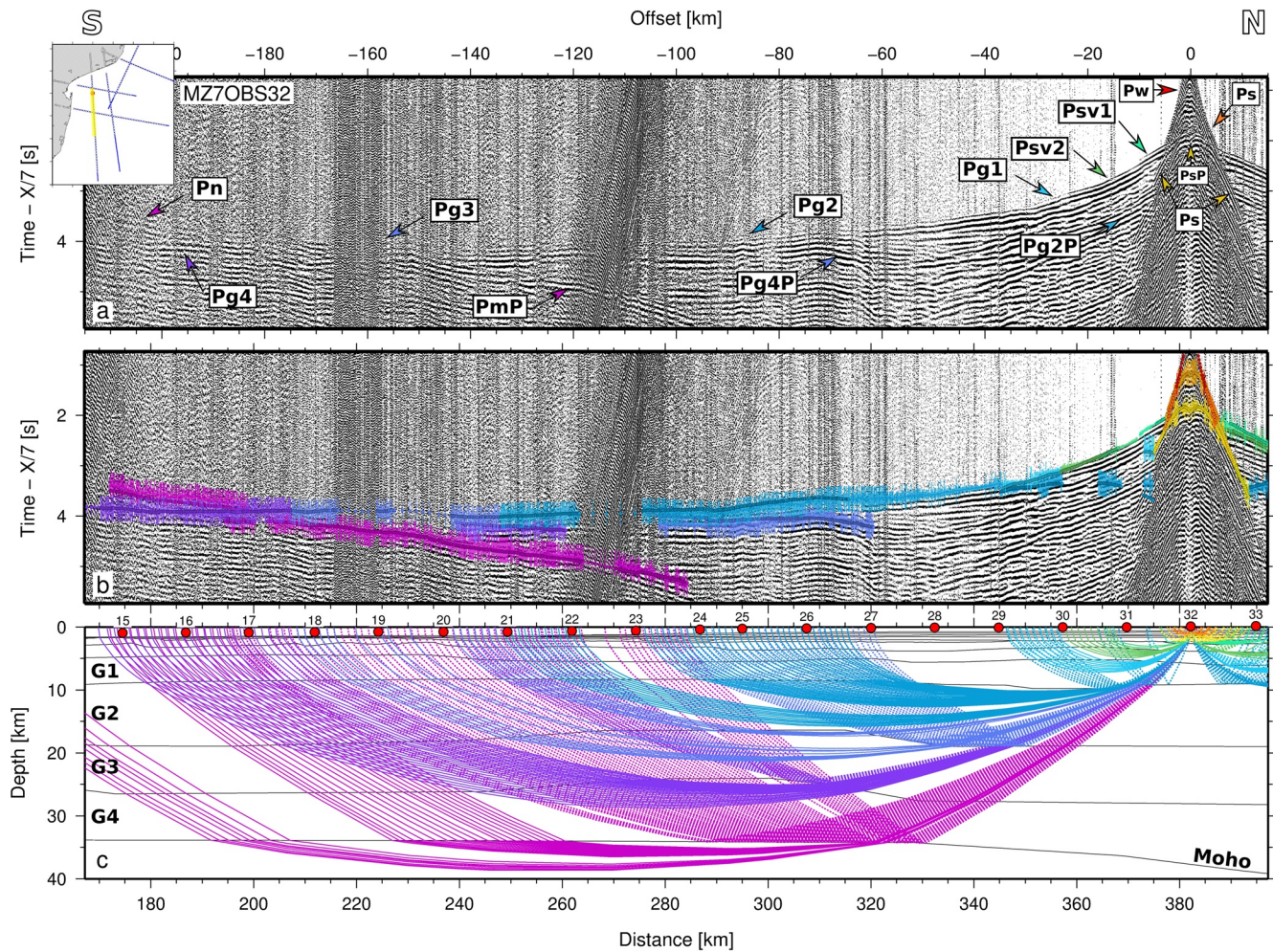


Figure 4. Data from MZ7OBS32 on MZ7 profile. (a) Geophone component of the recorded section with labels of the color-coded interpreted phases. A band-pass filter (4-6-32-48), a 7 km/s velocity reduction, and an offset-dependent gain are applied. (b) Geophone component of the recorded section with the color-coded observed travel-times picks (vertical bars, the size showing the uncertainty range), overlain by predicted travel-times in the final model (color-coded dots). (c) Model section showing corresponding ray-tracing.

Finally, the MZ7 model is parametrized by 18 different layers (Figures 7 and 8): the water layer, eight sedimentary layers, three volcano-sedimentary layers with intermediary velocities, four crustal layers and two mantelic layers. Water velocity was set to 1.51 km/s, the velocity used when correcting the OBS location for drift from the deployment position. The model depth node spacing in the sedimentary layer depends on the observed topography of the interfaces imaged on the seismic reflection record section. It logically increases with depth and is function of changes observed in the data and not necessary regular.

4.4. Model Evaluation

4.4.1. Error Analysis

The quality of the forward model can be quantified using the fit between predicted arrival times and travel-time picks, the number of ray traced in the model and the normalized chi-square. From MZ7 wide-angle data, we digitized 141767 events and interpreted their respective phase. Travel-time uncertainty was computed from the ratio of signal energy (in a 20 ms window) to average energy in the 68 ms preceding the signal according to Zelt and Forsyth (1994). The uncertainty ranges from 0.020 s for high ratio to 0.250 s for poor ratio. The model explains the travel-times and phase of 138750 events or 98% of total picks, with a global RMS travel-times residual of 0.050 s. The detailed fit statistics for each phase are given

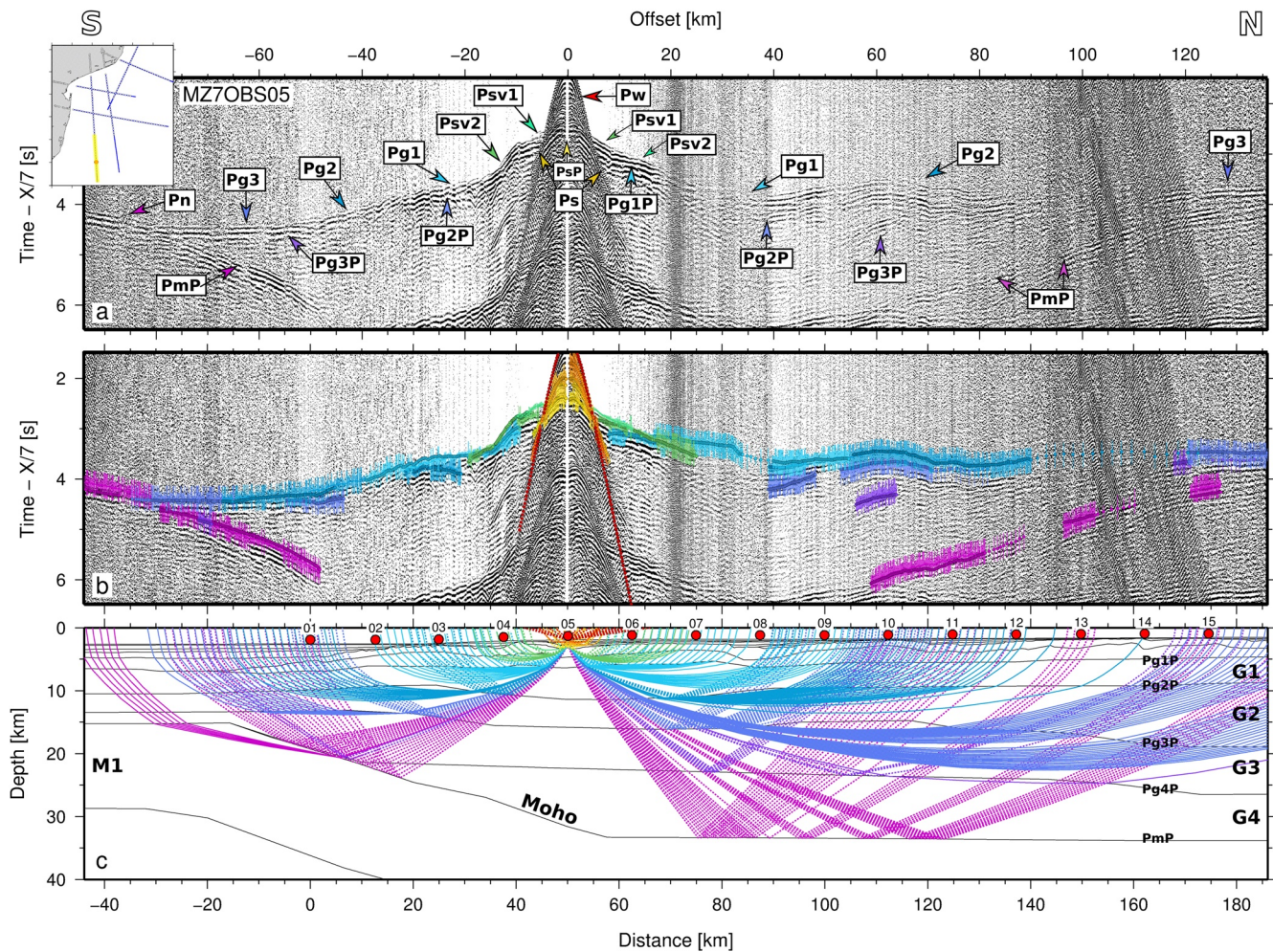


Figure 5. Data from MZ7OBS05 on MZ7 profile. (a) Geophone component of the recorded section with labels of the color-coded interpreted phases. A band-pass filter (4-6-32-48), a 7 km/s velocity reduction, and an offset-dependent gain are applied. (b) Geophone component of the recorded section with the color-coded observed travel-times picks (vertical bars, the size showing the uncertainty range), overlain by predicted travel-times in the final model (color-coded dots). (c) Model section showing corresponding ray-tracing.

in Table 1. We observe a general increase of the RMS from shallow to deeper phases, with a maximum between 0.084 and 0.110 s for the deepest phases from the upper mantle. Given our events individual calculated uncertainty, the model results in a low normalized chi-square of 0.322. Pg refracted arrivals represent the half part of the total events (with Pg1 8%, Pg2 28%, Pg3 10% and Pg4 4%), and Pm1P reflection at the Moho ~10%.

Figure 8c shows the model parametrization and the values of the diagonal of the resolution matrix for the velocity and depth nodes of the model. Interface depth node spacing as well as velocity node spacing is key to model the lateral variations of the seismic velocity with sufficient resolution, but without introducing complexity not required by the data. The resolution parameter is a measure of the number of rays passing through a region of the model constrained by a particular velocity node and is therefore dependent on the node spacing (Zelt, 1999). Ideally, these values are equal to 1. Nevertheless, values of the resolution matrix diagonals greater than 0.5 indicate reasonably well-resolved model parameters (e.g., Lutter & Nowack, 1990). Through the MZ7 model, the resolution parameter is calculated for the deepest layers not constrained by the MCS, from the top of SV2 to the upper mantle (Figure 8d). Resolution is generally very good, with values mainly higher or equal to 0.9. It tends to logically decrease at both extremities of the line where the ray coverage is less dense, and at the vicinity of high velocity lenses combined with underlying velocity inversions (resolution < 0.5), layer pinched-outs and low velocity layers.

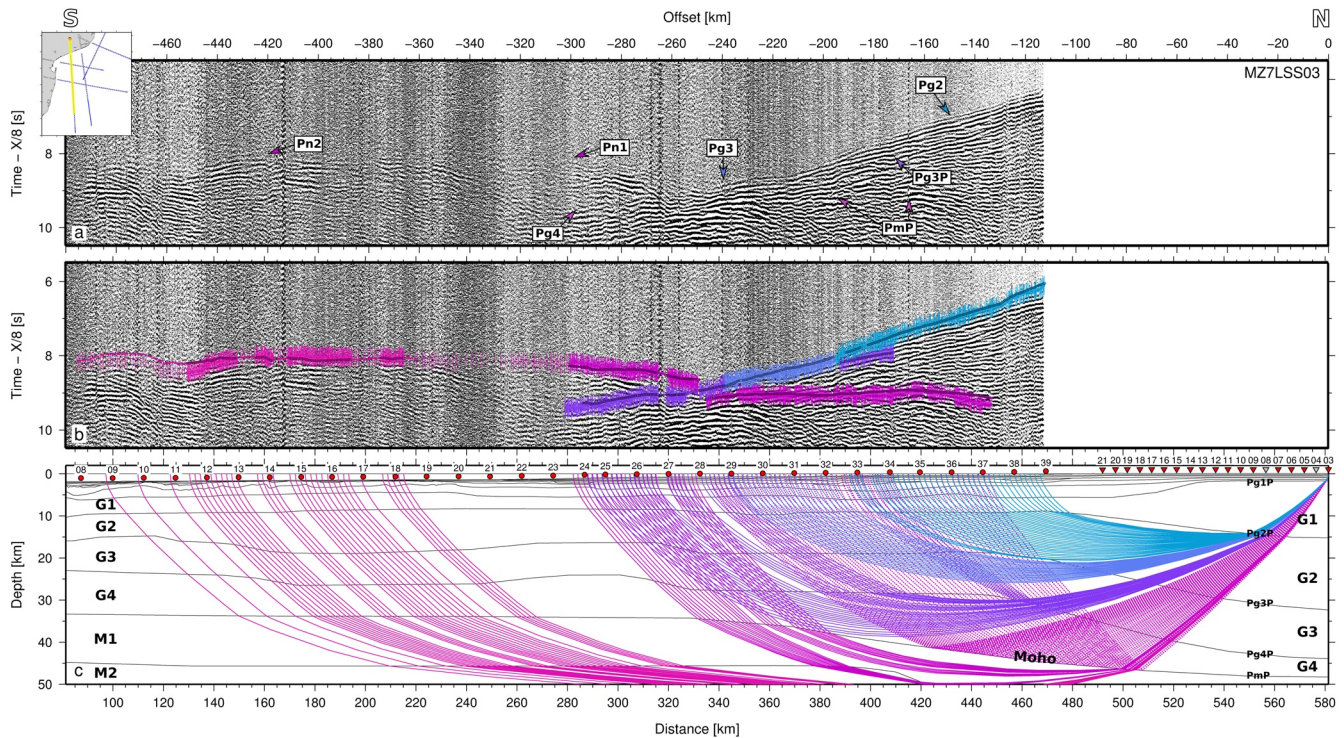


Figure 6. Data from MZ7LSS03 on MZ7 profile. (a) Vertical geophone component of the recorded section with labels of the color-coded interpreted phases. A band-pass filter (4-6-32-48), a 8 km/s velocity reduction, and an offset-dependent gain are applied. (b) Vertical geophone component of the recorded section with the color-coded observed travel-times picks (vertical bars, the size showing the uncertainty range), overlain by predicted travel-times in the final model (color-coded dots). (c) Model section showing corresponding ray-tracing.

4.4.2. Uncertainty Estimation Using VMONTECARLO

In order to assess model quality, uncertainty bounds and possible alternate solutions, we used the VMONTECARLO algorithm developed by Loureiro et al., (2016) based on a Monte Carlo approach. The code allows to test random direct XRAYINVR (Zelt & Smith, 1992) layered-models around a preferred model. Uncertainty assessment of a velocity model is of major importance (depths and velocities, minimum size of resolvable structures), since this will greatly impact the accuracy of geological interpretation.

For computational cost, the explored model space is reduce by limiting the number of parameters and fixing some bounds. In this sense, we have chosen to apply the Vmontecarlo process for the deeper crustal and mantelic layers only, and to maintain fixed the layers considered to be well constrained, that is, from the sedimentary sequence to the top of the crust. The depth nodes at the top of the crust are fixed while the 85 depth nodes forming the top of the layers G2, G3, G4 and M1 (Moho) are randomly displaced vertically. The velocity nodes are allowed to vary from the top of the layer G1 to the base of the upper mantel M1, for a total of 87 upper velocity nodes and 87 lower velocity nodes. Fifty thousand random models were generated with maximum velocity variations at each node of ± 0.4 km/s and maximum depth variations of ± 1.0 , 1.0, 2.5, and 3.5 km at the top of the layers G2, G3, G4 and M1 (Moho). Loureiro et al., (2016) defined an additional parameter ranging between 0 and 1, the model score, that is able to report on the quality of a model through its ability to predict the observations while maintaining good statistical fit. The first quality thresholds used to establish the model ensemble (ME) was set to 75% of the final model's quality of fit (75% of the final model score), together with thresholds of 80% explained picks, chi-square lower or equal to 2.0 and RMS lower or equal to 0.095 s. Since the quality score is constructed taking the log of the chi-square, our events individual (data driven) uncertainty was multiplied by 1.8 in order to obtain a final chi-square close to 1. This results in a normalized chi-square of our preferred model of 1.068, ensuring that all random model's scores are based on chi-square larger than 1. We finally obtained a score of 0.951 for our final model. For MZ7 on the 50,000 generated random models during the simulation, 46,735 models were valid (i.e., the ME), and 475 met the quality thresholds.

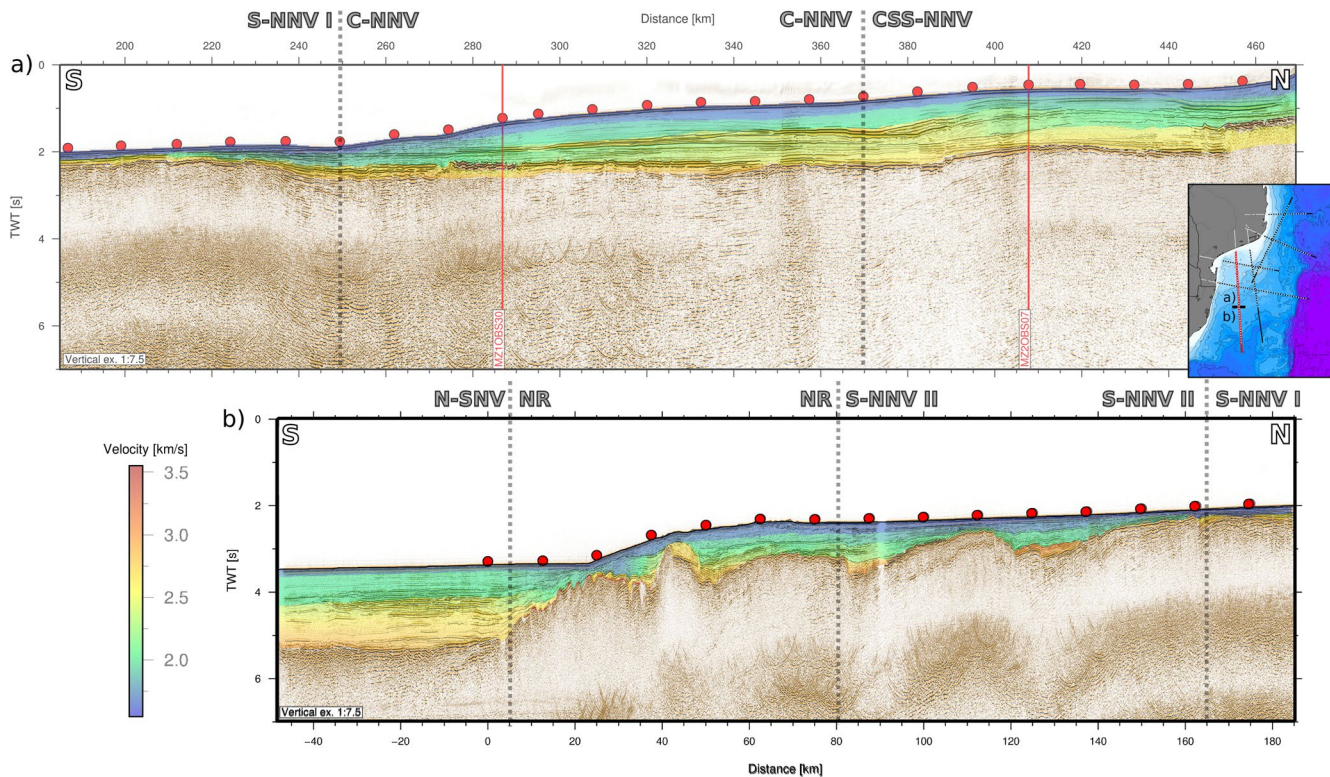


Figure 7. Two-way travel-time record section of MCS data along MZ7 profile overlain by time converted modeled P-wave velocities of wide-angle model in the upper sedimentary cover (velocities < 3.6 km/s). The intersections with the MOZ3/5 dataset are indicated by red line. OBS locations are indicated by red circle. Vertical exaggeration is 1:7.5. NNV, North Natal Valley; SNV, South Natal Valley.

These 475 random models were then used to build the global uncertainty map, representing the statistical maximum admissible interface depth and layer velocity increase/decreases along the MZ7 profile, and presented in Figures 9-I and 9-II. The final uncertainty is generally lower than ± 0.25 km/s except in the vicinity of the Moho where the final model presents the strongest velocity contrast. Note that the uncertainty found at the Moho between -50 and 10 km model-distance is mainly an artifact due to the presence of a pinch-out there in the final model (Figures 9-I & 9-II). Figure 9-III represents velocity-depth profiles extracted from each valid model at different positions along the wide-angle profile, and colored according to the normalized average model scores in the ME. In order to access uncertainty values for velocities or interface depths, horizontal and vertical cross-sections of the normalized average score distribution were extracted at different depths and velocities (colored lines, Figure 9b), and then represented in Figures 9a and 9c respectively. A threshold of 95% of the maximum normalized average score has been set in agreement with the result of the F-test study developed in Loureiro et al., (2016). These 95% confidence bounds are indicated by horizontal and vertical thin black dashed lines in Figures 9a and 9c, respectively. On Figure 9a, the crossing of the confidence bounds (horizontal black dashed line) with the normalized average score horizontal cross-sections (plain colored lines) allows us to read the uncertainty directly from the horizontal axis, highlighted by the vertical colored dashed lines for each horizontal cross-section. The same logic can be applied to Figure 9c in order to estimate the uncertainties of the interfaces depths as the possible occurrence of a specific velocity at depth.

Vertical slices through the model space are extracted where the normalized scores of the 50,000 random models are plotted, together with four slightly adapted depth profiles according the position along the profile, and five constant velocity profiles (6.3, 6.8, 7.0, 7.3 and 7.9 km/s) and their respective 95% confidence bounds. Locally, one adaptive velocity profile (from 7.1 to 7.5 km/s) could be added as a function of the velocity variations away from the central 7.3 km/s velocity at the base of the crust along the line.

Table 1
MZ7 Reflected or Refracted Phase Names and Their Associated Number of Explained Events (N), RMS Misfit Between Calculated and Picked Travel Times (tRMS, s), and Normalized Chi-Square Value (χ^2)

Phase	N	tRMS (s)	χ^2
Pw	4587	0.015	0.123
Ps1	123	0.007	0.055
Ps2P	307	0.026	0.022
Ps2	514	0.012	0.156
Ps3P	1049	0.025	0.1
Ps3	130	0.018	0.297
Ps4P	532	0.02	0.074
Ps4	932	0.015	0.268
Ps5P	1669	0.019	0.078
Ps5	31	0.016	0.105
Ps6P	25	0.013	0.021
Ps6	613	0.02	0.217
Ps7aP	2539	0.022	0.083
Ps7a	58	0.022	0.359
Ps7bP	22	0.029	0.123
Ps7b	43	0.021	0.176
Psv1aP	376	0.019	0.032
Psv1a	346	0.021	0.337
Psv1bP	139	0.054	0.366
Psv1b	2657	0.022	0.543
Psv2P	2376	0.043	0.34
Psv2	5295	0.031	0.544
Pg1P	3009	0.046	0.289
Pg1	11381	0.037	0.49
Pg2P	4712	0.052	0.284
Pg2	39724	0.045	0.214
Pg3P	8437	0.056	0.257
Pg3	14932	0.042	0.124
Pg4P	6526	0.081	0.542
Pg4	5346	0.051	0.205
Pm1P	14567	0.084	0.527
Pn1	1297	0.087	0.45
Pm2P	3495	0.11	1.141
Pm2	961	0.643	0.643
All phases	13750	0.053	0.021

To illustrate the approach, we propose to use the example of the evolution of the normalized model score at 500 km model-distance around the Moho interface (Figure 9a). We observed that at 40 km depth (pink line EF) the velocities can vary between 7.05 and 7.09 km/s without reducing the average model scores by more than 5%, whereas at 47.5 km depth (orange line GH) they can vary between 7.88 and 7.94 km/s. By contrast on Figure 9c, the mantle velocities of 7.9 km/s (magenta line ST) and the Moho interface can vary between 46.5 and 48.21 km depth without large changes in model quality, whereas velocities of 7.10 km/s give the highest score between 42.36 and 45.84 km depth, just above the Moho. Furthermore, vertical cross-sections for the velocities from 6.8 to 7.1 km/s further attest of the particularly low velocity gradient North of the line.

Finally, the horizontal cross-sections (panels a) show a good constraint of the velocity field at their respective depths, since the width of the 95% confidence velocity bound rarely exceeds ± 0.05 km/s. At all local analysis locations, random velocity variations larger than about ± 0.150 km/s all lead to scores lower than 0.25 (panels b). Our final model (black line, panels b) that follows the orange to red valley formed by the best normalized scores values, attests of the good quality of our solution. It is slightly degraded at the southern edge of the model for the Moho at 0 km model-distance mostly due to the difficulty for the Vmontecarlo code to take into account the pinch-out between the interface at the top of G4 and the one at the top of M1.

5. Velocity Model & N-S Structure of the South Mozambique Region

In this study we analyzed the deep seismic profile MZ7 crossing in a N-S direction the Mozambique Coastal Plain, the North Natal Valley and the northern extremity of the South Natal Valley. The MOZ3/5 wide-angle data combined with the coincident MCS allow us to define the overall geometry of the South Mozambique margin along the MZ7 line, that images the geometry of sedimentary (S), volcano-sedimentary (SV), crustal (G), and mantle layers (M) to a depth of around 55 km (Figure 7 and 8). The deepest layers (G1, G2, G3, G4, M1 and M2) are interpreted from the wide-angle data and are not imaged on the MCS profile. We separately describe in a first time the velocity modeling for the sedimentary and SV sequences, in a second time, the crustal layers according to the resulting refined segmentation of crustal domains.

5.1. Sedimentary Layers Structure

A total of eight sedimentary layers are included in the modeling, with numerous pinch-outs along the profile, from the shallower modeling layer labeled S1 to the deepest one S7b (Figure 2). The upper sedimentary sequence includes two thin local high velocity lenses (S5 and S7a) responsible of velocity inversions indicated by typical seismic signal gaps

on OBS data (Figure 3). In the NNV, the whole sedimentary sequence reveals a maximum thickness of ~ 1.8 km North of the MCS line (~ 385 – 390 km model-distance) through the Limpopo Cone, and a minimum of less than 0.3 km at the Central Terrace (Figures 2 and 8b). Furthermore, as the sedimentary layers thin approaching the Central Terrace, an important decrease of the velocities is observed through all the layers. Figure 7 illustrates this observation focusing on the P-waves velocity model converted in time for the

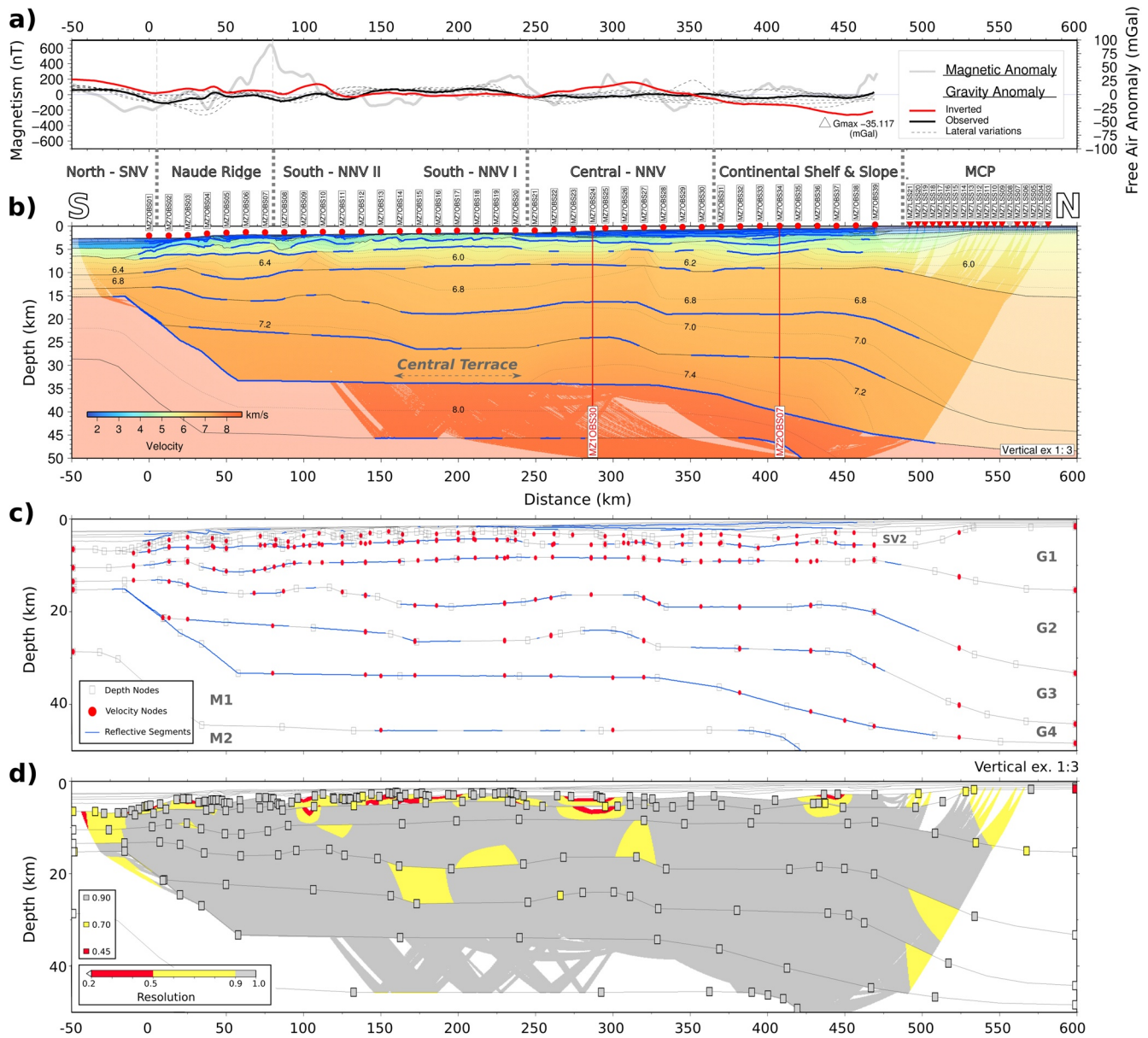


Figure 8. Final velocity model for the MZ7 profile and evaluation of the wide-angle model. (a) Observed (BGI) and inverted gravity anomalies are indicated by the solid black line and the solid red line respectively. The thicker gray line is the magnetism along the profile (EMAG2). (b) Final MZ7 velocity model. Thick blue lines indicate interfaces constrained by wide-angle reflections. Shaded areas indicate ray-coverage. (c) Model parameterization, including interface depth nodes (squares), top and bottom layer velocity nodes (red circles). Interfaces where reflections have been observed on OBS/LSS data are highlighted in blue. (d) Resolution of velocity (gridded and colored) and depth nodes (colored squares). Zones that were not imaged are blanked. MCP, Mozambique Coastal Plain; NNV, North Natal Valley; SNV, South Natal Valley.

upper sedimentary cover (<3.6 km/s). Then, in the N-SNV, the sedimentary sequence reaches its maximum thickness along MZ7, with a regular thickness of ~ 2.25 km.

In the NNV, the uppermost mainly transparent ensemble S1/S2, including a relative high velocity lens part of the modeling layer S3 at its base to the North, lies in unconformity on the S4 or S6 layers (Figure 2, at 255–375 km model-distance). This is indicated on MZ7 MCS by down-laps and high amplitude reflectors at the contact, that correlate well with a prominent reflection on the OBSs (Figure 3). S1 and S2 present very low top and bottom velocities from 1.60 to 1.75 km/s and 1.75–2.05 km/s respectively (Figures 2 and 4). The S3 layer has top-bottom velocities in the range of 1.70–2.20 km/s in the S-NNV, whereas on the continental shelf the S3 lens only corresponds to an area of slightly higher velocities in the range of 2.20–2.70 km/s,

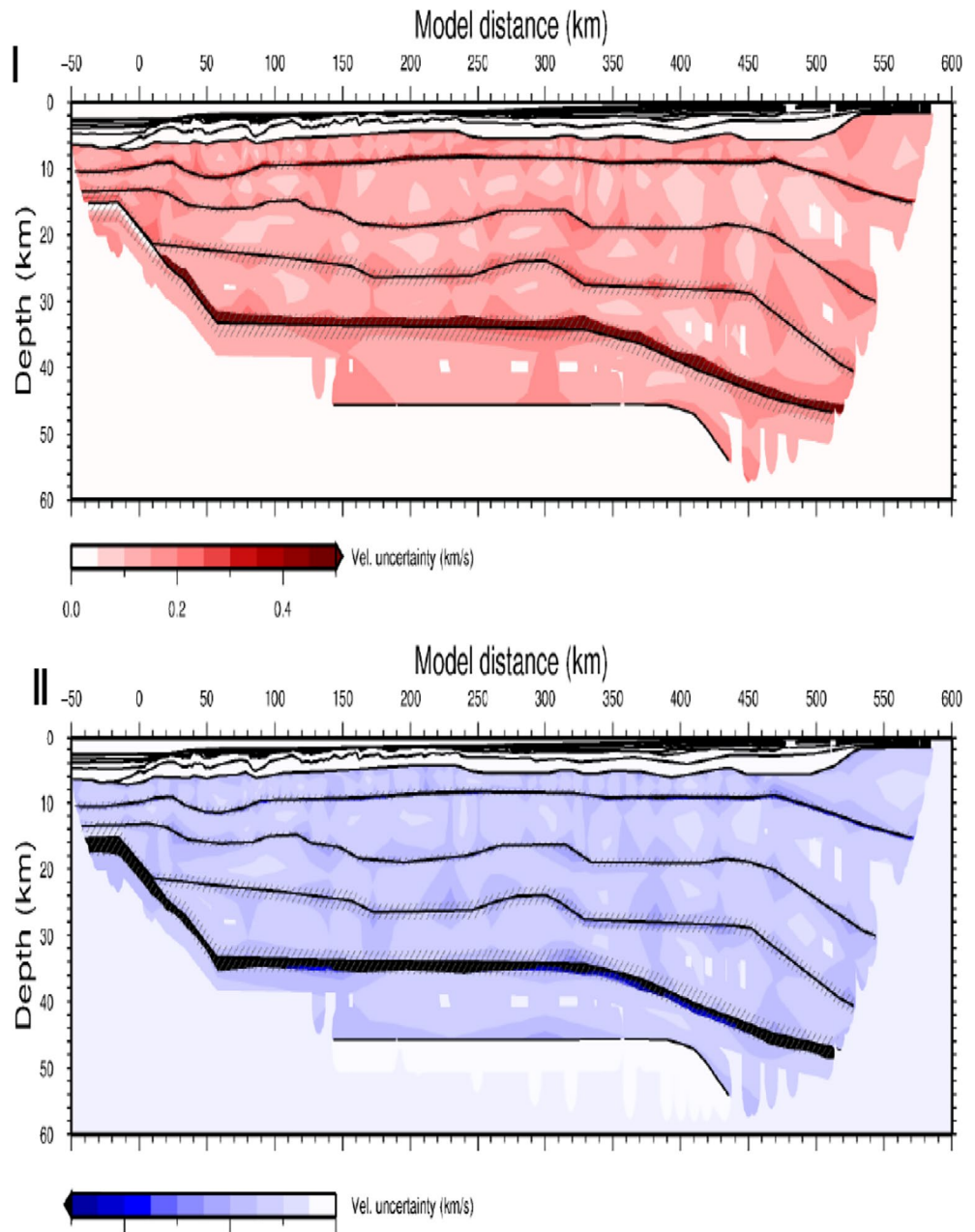


Figure 9. I–II: Global uncertainty map generated from the standard deviation of the 475 random models meeting our thresholds. Crust and mantle portion of our final wide-angle model MZ7. (I) Positive velocity uncertainty. (II) Negative velocity uncertainty. The hashed areas indicate the standard deviation of the depth of the interfaces explored during Vmontecarlo. III–Evaluation of the wide-angle model MZ7 through the normalized average scores distribution at 500, 450, 300, 150, 50 and 0 km model-distance. (b) Normalized average model scores distribution. Black line indicates the final velocity model. Thin dashed black envelope indicates the exploration domain of independent parameter uncertainties. Colored lines mark the location of horizontal (constant depth, letters A to H) and vertical (constant velocity, letters K–V) cross-sections of the average model scores presented in (a) and (c) respectively. Thick black dash-lines on (a) and (c) indicate the 95% of confidence level, that is, 95% of the normalized average score.

responsible of a velocity inversion at its base (Figures 2 and 4 at 285–360 km model-distance). This is revealed on the reflection seismic by an increase in amplitude of the reflectors, probably reflecting a more sandy area. At the northern extremity of the line, the S5 high-velocity lens (450–470 km model-distance) shows top-bottom velocities in the range 3.50–4.35 km/s. It typically coincides on the MCS data with the high amplitude and rough facies mentioned above, combined with a major loss of the seismic signal below

III

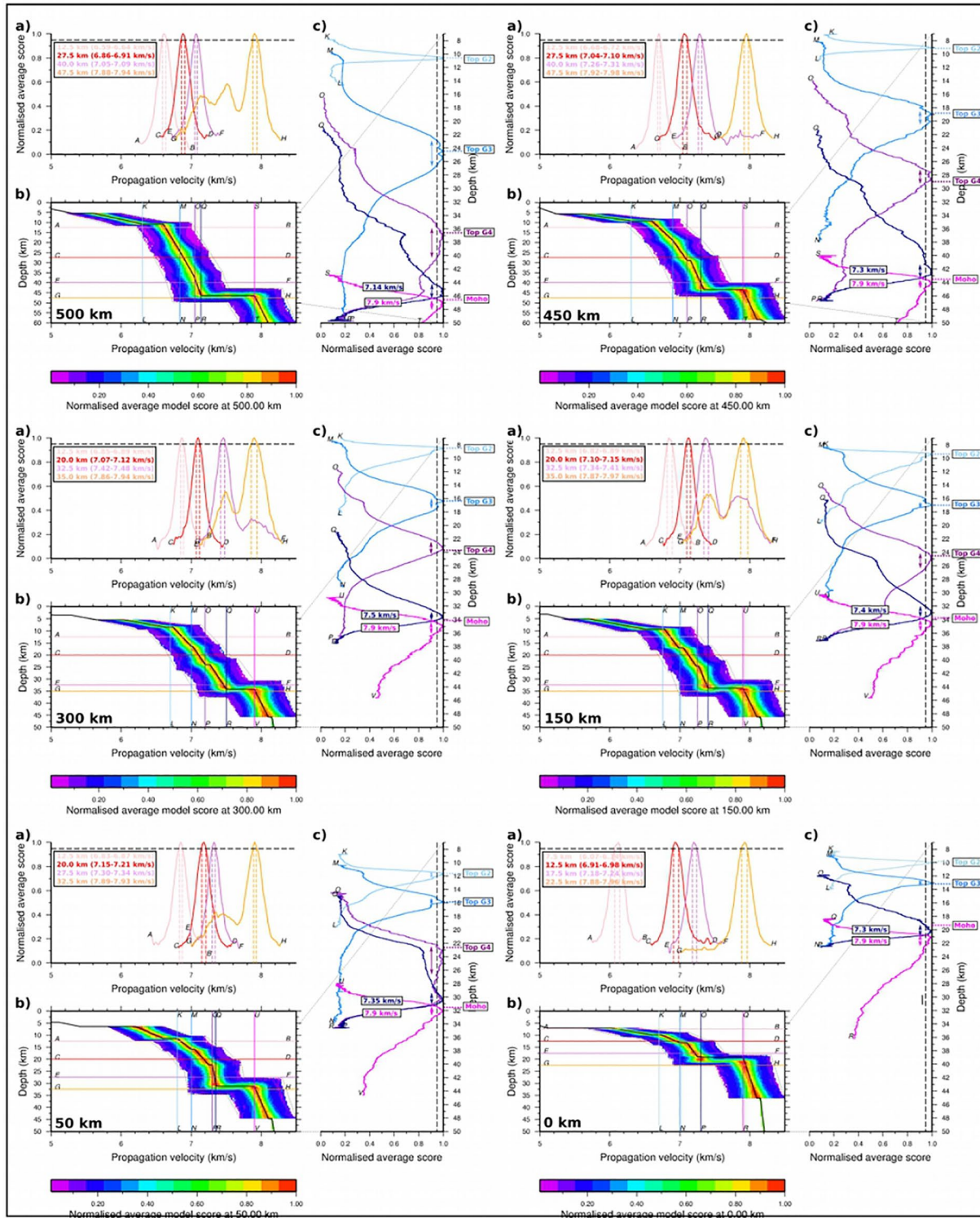


Figure 9. Continued.

(Figure 2). The underlying S4 and S6 layers show large range of top-bottom velocities, mainly between 2.1–2.2 km/s and 2.4–2.5 km/s for S4, and 2.25–2.60 km/s and 2.55–3.25 through S6 North and South of the Central Terrace, respectively. The local high velocity lens S7a (275–290 km model-distance) at the top of the

S7b layer show slightly higher velocities than the S5 lens, in the range 3.80–4.50 km/s. It is further highlighted on the MCS, having the same seismic characteristics as S5. Below, the latest modeling S7b layer modeled North of the profile and along the Central Terrace, shows velocities from 2.40 to 2.80 km/s (Figures 2 and 4).

Finally, in the N-SNV (-50-0 km model-distance) the four modeled sedimentary layers all show a very regular thickness, with top-bottom velocities in the range of 1.65–180 km/s for S1, 1.85–2.05 km/s for S2, 2.08–2.50 km/s for S4 and 2.55–2.90 km/s for S6 (Figures 2 and 4).

5.2. Volcano-Sedimentary Layers Structure

Between the sedimentary sequence and the crystalline crust, two major layers are used to model the volcano-sedimentary sequence: the SV1b layer generally corresponding to the last coherent layer on MZ7 MCS, and the deepest one labeled SV2 that never exceed velocities of 6 km/s (Figures 2 and 4). The shallower layer SV1a is only included to take into account three local high velocity lenses with velocities between 4.55 and 4.85 km/s, and their associated velocity inversions. The top of the volcano-sedimentary sequence presents important lateral changes in the seismic signature of the preeminent reflector (Figure 2, The SV1b and SV2 layers are modeled with thicknesses around 1–1.25 km and 1.75–2.00 km respectively, resulting in an average thickness around 3–3.25 km of volcano-sedimentary to volcanic materials considering the whole SV sequence (Figure 8b). In the NNV, the SV1b and SV2 layers are characterized by velocity ranges from 3.50 to 5.20 km/s and 4.70 to 6.00 km/s, respectively. In the N-SNV, the SV1b layer has top-bottom velocities of 5.00–5.30 km/s, whereas the SV2 layer is absent.

All these characteristics reveal the non-uniformity of at least the SV1 layer through which the signal vanishes on MZ7 MCS, and probable variations in the volcanic/sedimentary ratio laterally and with depth. The importance of volcanic activity in the area is further illustrated by the high velocities lenses well expressed on the reflection and refraction seismic data (Figure 3) revealing the presence of inter-bedded volcanic sills through the sedimentation cover or at the top of the SV sequence. Furthermore, the different positions of the sills through the sedimentary sequence notably North of the line reflect the occurrence of several magmatic events through the time in the NNV.

5.3. Crustal Structure

From the MCP to the Naude Ridge, the basement is modeled using four layers (G1–G4). The transition from the SV sequence to the true crystalline crust may be sometimes difficult to discern in the absence of a strong velocity contrast between the two, especially below the MCP. The number of crustal layers used in the NNV is due to themore or less pronounced intra-crustal reflections identified on the wide-angle data, and/or changes in the seismic signal of the refracted arrivals. Combining the seismic observations from the MZ7 profile and the other lines from the MOZ3/5 dataset, we draw a coherent segmentation of the crustal architecture South Mozambique (Moulin et al., 2020). It results along MZ7 in three main domains and five sub-domains part of the NNV, from North to South: (1) the MCP, (2) the NNV, including the Continent Shelf & Slope (CSS-NNV), the Central – North Natal Valley (C-NNV), the South – North Natal Valley (S-NNV I and II), and the Naude Ridge (NR-NNV), and finally (3) the North – South Natal Valley (N-SNV).

5.3.1. Mozambique Coastal Plain (MCP)

In the onshore domain of the MCP (~485–600 km model distance), basement velocities in the northernmost portion constrained by ray-tracing are of 5.60–6.30 km/s, 6.60–6.80 km/s, 6.90–7.00 km/s, and 7.00–7.10 km/s in the layers G1, G2, G3 and G4 respectively (Figures 8 and 9 at 500 km). The vertical velocity structure results in relatively homogeneous and very low velocity gradients from 0.05 to 0.06 km/s/km in G1 to 0.015 km/s/km in the deeper layers. Then, velocities tend to progressively increase southwards, mainly at the base of the crust. Due to the absence of reversal shots on land and the absence of recorded refracted and reflected arrivals from the uppermost layers, the geometry of the layers in the 5–10 first kilometers in the southern part of the MCP is relatively uncertain, although the position of the velocities at depth is better constrained, at least near the coast (Figure 9b at 500 km model-distance). Indeed, the lack of recorded sedimentary arrivals or reflections at the top of the crust onshore, combined with the presence of high-velocities SV layers (up to ~6 km/s) leave some doubts on the exact position of the top of the crystalline crust below

the MCP. The upper part of the G1 layer could include a part sedimentary to volcano-sedimentary materials. Furthermore, the Moho discontinuity lies at great depths between 48 and 45 km, with decreasing depths toward the South. Considering the doubts on the position of the top of the true crystalline crust, it would nevertheless indicate a crust at least 35 km thick, probably between 35 and 40 km.

5.3.2. North Natal Valley (NNV)

Offshore, the NNV (~5–490 km model-distance) globally presents an atypical velocity architecture, with an average total crustal thickness around 30 km. A large portion of crustal velocities are faster or equal to 7.0 km/s (15 and 18 km thick) and characterized by low velocity gradients mainly between 0.01 and 0.04 km/s/km. The highest velocity gradients are found in areas of velocity intrusions. The NNV reveals several lateral variations in its velocity structure that highlight different sub-domains. The resulting sub-segments are presented here with the specificities of each domain and the passage from a segment to another.

Continental Shelf & Slope (CSS)

In the northernmost part of the NNV, the domain CSS (370–490 km model-distance) exhibits an internal velocity structure of the upper and middle crust relatively similar to the domain MCP. Velocities gently increase of ~0.1 km/s at the base of the layer G2 (6.6–6.9 km/s) and at the top and the bottom of the layer G3 (6.9–7.1 km/s) from 520 km model-distance to 470 km, and remains unchanged along the whole CSS, except for some local increases at the top of G1 in the range 5.6–6.0 km/s. The main differences lie in 1) the rise of the intra-crustal interfaces to shallower depths and 2) the architecture of the lower crustal layer G4, with the southwards increase of its top-bottom velocities to 7.2–7.5 km/s and its thickening (at 500 and 450 km model-distance, Figure 9). The Moho gently rises toward the South from ~45 to ~35 km depth with a moderate thinning of the crust, from 480 to 370 km model-distance.

Central - North Natal Valley (C-NNV)

By contrast, the domain C-NNV (250–370 km model-distance) corresponds to an area of higher crustal velocities, which clearly increase in all the crustal layers, and locally in the SV sequence (Figure 8). Velocities at the top of the crust reach 5.8–6.5 km/s, while velocities at the base of the crust remain fixed at 7.5 km/s (at 300 km on Figure 9). The presence of an increment in velocity at shallower depths is further illustrated by the rise of the modeled interfaces, mimicking a dome-shape high velocity structure. The Moho runs at about 34 km depth, for a total crustal thicknesses of ~30 km.

South - North Natal Valley I (S-NNV I)

Directly South of the C-NNV, the sub-domain S-NNV I (165–250 km model-distance), including the Central Terrace, has upper and lower crustal velocities compared to the surrounding C-NNV and the S-NNV II areas (Figure 8). It exhibits decreasing velocities of 5.7–5.8 km/s and 7.3 km/s at the top and the bottom of the crust respectively. The tops of SV and the crust appears closer to the seafloor and the upper sedimentary cover very thin. Nevertheless, the crustal thickness and the Moho depth remain relatively stable from the C-NNV to S-NNV II.

South - North Natal Valley II (S-NNV II)

Similarly to the C-NNV, the S-NNV II sub-domain (85–165 km model-distance) is characterized by crustal velocities from 5.7–6.5 km/s at the top to 7.4 km/s at the bottom (Figure 8). From 115 km model-distance to the southern limit of the NNV (~5 km model-distance), a general increase of the crustal velocities is observed and no velocities lower than 6 km/s are recorded by the crustal phases, which differs from what of the dome-like geometry in the C-NNV. The southwards rise of the interfaces reflects the position of high velocities at shallower depths and probably an incipient thinning of the upper/middle crust, while the high velocity lower crustal layer G4 (7.3–7.4 km/s) thickens.

Crustal scale deformation, magmatism and faulting are highlighted by the complex seismic structure of the 2 first kilometers below the seafloor in the area on the MCS (Figure 10), and the general tendency to dip southwards South of the Central Terrace. That agree with the overall thickening of the sedimentary cover southwards through the sub-basins above SV, from North to South (~1.0–1.7 km thick). The identification of southwards-dipping (or seawards-dipping) reflectors series through the SV sequence (4.0–4.8 km/s), particularly between 85 and 100 km model-distance (Figure 10) just North of the Naude Ridge sub-domain,

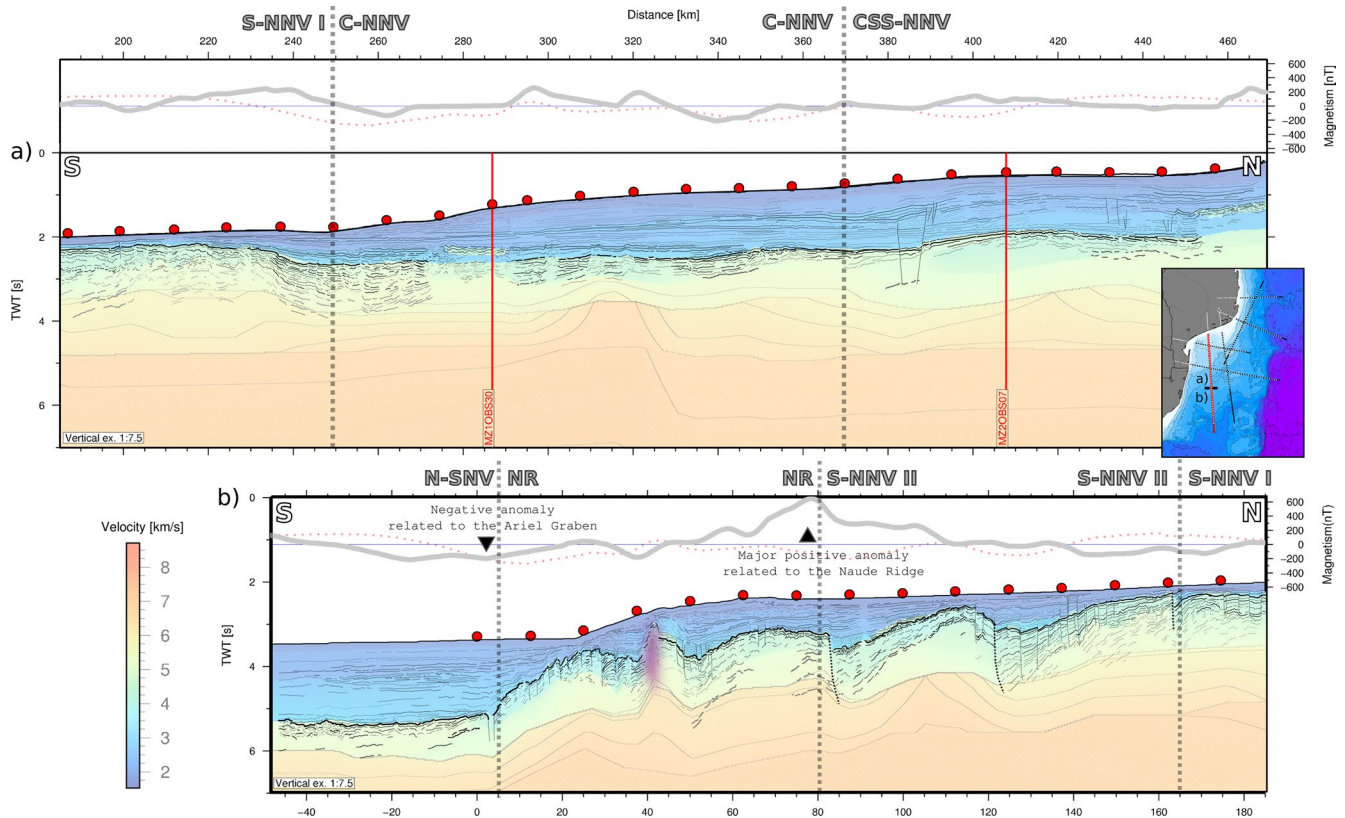


Figure 10. Time converted wide-angle P-wave velocities model overlain by the interpretative line drawing of the two-way travel-time record section of MCS data along MZ7 profile. The intersections with the MOZ3/5 dataset are indicated by red line. OBS locations are indicated by red circle. Upper panels in (a) and (b) show the magnetism (thick gray line, EMAG2) and the trend of the observed gravity anomaly (dash light red line, BGI) along the profile. Purple color: youngest evidence of Magmatism. Vertical exaggeration is 1:7.5. NNV, North Natal Valley; NR, Naude Ridge; SNV, South Natal Valley.

seems to indicate fan-shaped sedimentation mixed with volcanic material, located between 10–15 km wide morphological high.

Naude Ridge (NR)

At the southern extremity of the NNV (5–85 km model-distance), the domain NR, including the Naude Ridge structures, is marked by a major crustal thinning reducing the crust to about 20 km (Figure 8). The crustal seismic velocities are between 6.0–6.2 km/s and 7.4 km/s from G1 to G4. The passage from the S-NNV is marked by a strong positive magnetic anomaly (~600 nT, Figures 8 and 10) typically correlated with the NR in the literature (e.g., Mueller & Jokat, 2019), and coherent with the higher velocities and an highly intruded crust in the South part of the NNV considering the entire crustal column. Furthermore, deep low amplitude reflectors (~4–5 s twt) of relative higher amplitude are imaged on the MCS at the location of the magnetic peak, which may support the presence of additional magmatic intrusion (Figures 4 and 10). Between 40–50 km model-distance, the upper sedimentary cover is clearly deformed and intruded by post-sedimentary magmatism (purple intrusion, Figure 10), that seems to be injected along pre-existing structures at the junction of tectonised blocks. Between km 15 and 40, reflectors below the SV top appear delayed and highly faulted which could explain the decrease in velocity through the layer to 3.5–4.2 km/s, against 4.1–4.8 km/s North of km 40.

5.3.3. North–South Natal Valley (N-SNV)

The N-SNV domain (-50–5 km model-distance) presents a much thinner crust than the one underlying the NNV (Figure 8). The crustal thinning along the Naude Ridge sub-domain results in a reduced crustal

thickness to around 8 km at the southern extremity of the MZ7 line, depending on whether or not the extension of the layer SV1 (5.0–5.3 km/s) is included as part of the basement. The deepest layers G1, G2 and G3 are modeled with top-bottom velocities of 6.0–6.6 km, 6.7–7.0 km/s, 7.1–7.25 km/s respectively. The lower crustal layer G4 is absent there since it pinches-out at the transition from the NR to S-NNV, which seems to indicate a major change in crustal/tectonic domain. The presence of high velocities in the range of 7.3–7.5 km/s as observed in the NNV is not supported in the N-SNV (0 km model-distance, Figure 9).

At shallower depths, the transition N-SNV/NNV is revealed through a buried morphological high formed by the top of the modeled SV sequence before it appears smoother and flat south at km 0–5 (Figure 10). Indeed, the MZ7 MCS line shows a clear slope-break of the top SV interface south of the NR, that appears shifted with respect to the current slope-break at the seafloor, and the seismic facies below the interface radically changed (Figure 2). The meaning of the SV modeling sequence clearly change arriving in the N-SNV. The limit NNV/N-SNV is further indicated by negative magnetic and gravity anomaly, related to the SW-NE oriented Ariel Graben (Figures 1 and 10).

Unfortunately, whilst we have good constraint on the crustal thinning at the southern portion of the NNV which represents a necking zone, the SNV begins where our profile ends and the constraints on the crustal structure are there limited (Figure 8). As mentioned above, the thickness of the crust is there mostly constrained by the relatively short offset Pn refracted arrivals on the OBS data (Figure 6).

5.3.4. Upper Mantle

Finally, the modeled upper mantle top-bottom velocities are constant along the entire profile, with 7.9–8.1 km/s in the upper layer M1 and 8.15–8.25 km/s below in M2. The interface between M1 and M2 is inserted due to local deep upper mantle reflections on wide-angle data and to manage velocity gradients (Figure 8).

6. Discussion

Due to the lack of deep seismic data, the crustal nature of the MCP and the NNV was largely controversial and speculative, although it is crucial in the understanding of the early stages of the Gondwana break-up in plate reconstructions. Mainly based on potential fields studies and kinematic models, the interpretations of the crust flooring the MCP and the NNV are very contrasted in term of nature, from oceanic to continental or transitional crust, and of estimated crustal thicknesses (e.g., Darracott et al., 1974; Domingues et al., 2016; Goodlad et al., 1982; Hanyu et al., 2017; Leinweber et al., 2011; Mueller & Jokat, 2019; Tikku et al., 2002). The compositions of the MCP and the NNV are crucial in restoring Africa-Antarctica-South America plate movements since they control the determination of the location of continent-ocean boundary (COB) SE Africa. The present study therefore provides key data to discuss the ~N-S South Mozambique crustal segmentation, the crustal nature of each segment, the position of the COB or at least the necking zone, and the possible meaning of the more local structures of the Naude Ridge and the Ariel Graben.

For that purpose, velocity-depth profiles were extracted every 10 km along MZ7 (Figure 11a), and then compared to the compilations for Atlantic-type Oceanic Crust from White et al. (1992) and for Continental Crust from Christensen and Mooney (1995).

6.1. Nature of the Crust Below the MCP

The crustal thickness in the range 35–40 km modeled below the MCP (at least >35 km) directly rises the question of the possibility of an oceanic nature of the crust there: a normal oceanic crust has a mean thickness of 7.1 ± 0.8 km, White et al., 1992) and oceanic plateaux are much less thick. The Ontong Java Plateau could reach ~33 km or slightly more (Miura et al., 2004) but this plateau appears rather as an exception (Tetreault & Buitier, 2014). Our values obtained for the southernmost part of the MCP are higher than the crustal thickness of 20–30 km from the recent passive seismic survey conducted N-NE of the MZ7 profiles in the MCP (Domingues et al., 2016, see location, Figure 1). Their estimations are derived from two 1-D Vp-depth profiles extracted at the points 1 and 2 shown on Figure 1, near the coastline and in the Mazenga Graben respectively. Differences in geographical positions may explain the discrepancy between the values,

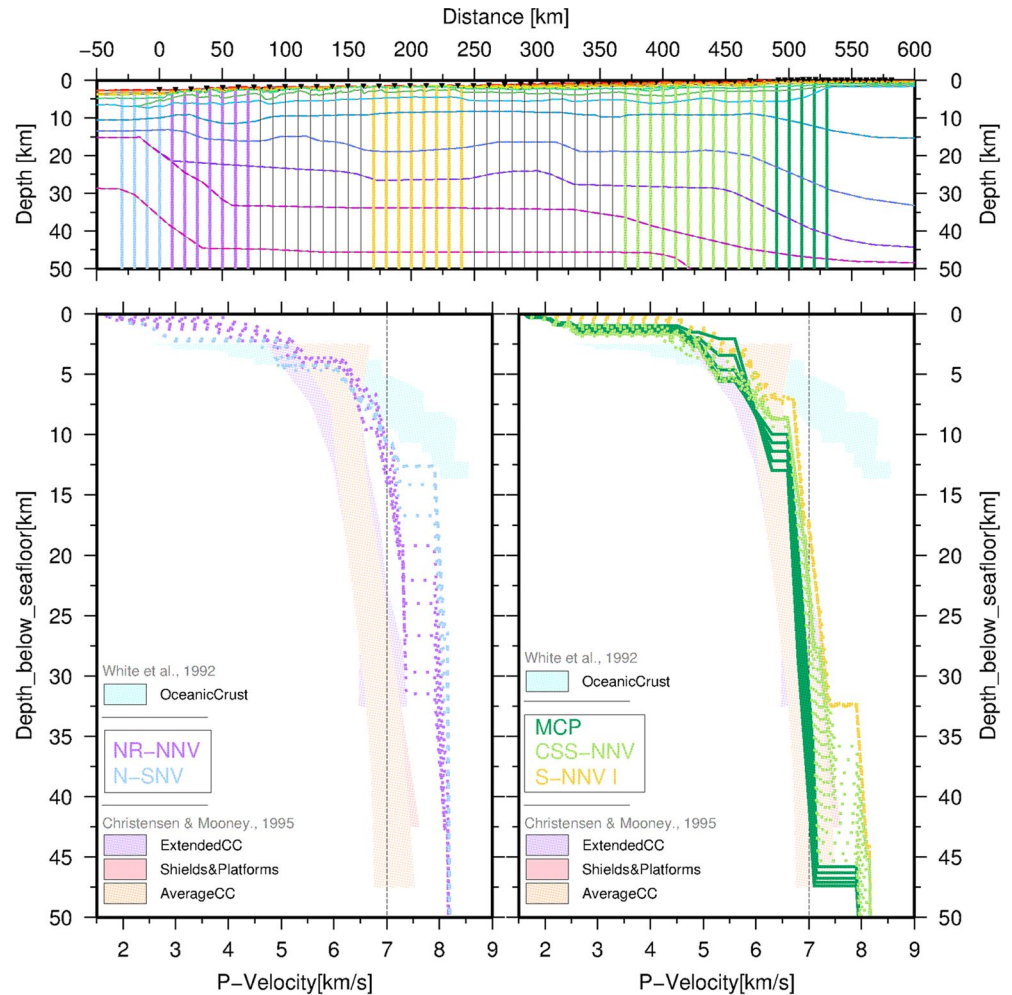


Figure 11. Comparison of the 1-D velocity-depth profiles (1D velocity profiles) extracted from the final P-waves velocity model for different domains along the MZ7 line with compilations from the literature. (a) Distribution of the 1-D velocity-depth profiles extracted and presented in (b) and (c). The color-code is according to the segmentation along MZ7. (b) Comparison of the 1D velocity profiles extracted in the MCP domain and the CSS and the S-NNV sub-domains with the compilation for ContinentalCrust (CC) from Christensen & Mooney, 1995. (c) Comparison of the 1D velocity profiles extracted in the N-SNV domain and the NR sub-domain with the compilation for Atlantic Oceanic Crust from White et al., 1992. CSS, Continental Shelf & Slope; MCP, Mozambique Coastal Plain; NNV, North Natal Valley; NR, Naude Ridge; S-SNV, North – South Natal Valley.

as well as the unclear thickness of sedimentary and volcanic materials in the approximately first 10 km at depth combined with the uncertainty on the Moho location from the 1-D V_p -depth curves. Finally, these authors also discard the possibility of oceanic crust flooring the MCP due to the combination of slow S-waves velocities, the important depth of the Moho and crustal thickness, and the thinning of the crust toward the East from point 2 to 1. Alternatively to oceanic crust, they propose a possible transitional crust from continental to oceanic, considering an W-E direction.

Velocities in the upper (5.6–6.3 km/s) and lower (up to 7.1 km/s) crusts at the MCP clearly contrast with velocity gradients found for oceanic crust of $\sim 1.0 \text{ km}^* \text{ s}^{-1} / \text{km}$ in the upper crust and $0.1\text{--}0.2 \text{ km}^* \text{ s}^{-1} / \text{km}$ in the gabbroic lower crust (Christeson et al., 2019; Grevemeyer et al., 2018; White et al., 1992), as with the general velocity-depth profiles trend of the compilation for Oceanic Crust as shown in Figure 11b.

In order to test the hypothesis of the presence of a thick oceanic crust, Moulin et al. (2020) have compared the 1D velocity-depth profiles of MCP to the 1D velocity-depth profiles of some peculiar thickened oceanic structures like the Agulhas plateau (Gohl & Uenzelmann-Neben, 2001), the Ontong Java Plateau (Miura

et al., 2004), the South Mozambique ridge (Gohl et al., 2011), the Kerguelen plateau (Charvis & Operato, 1999) or the Tuamotu plateau (Patriat et al., 2002). None of these structures, characterized by a 4–9 km thick upper layer with very low velocities (4–5 km/s at the top) typical of the first layer of oceanic crust, match the NNV velocity distribution (Moulin et al., 2020).

In contrast, the 1D velocity-depth profiles are coherent with those of average Continental Crust at 5 km depth about 5.95 ± 0.73 km/s, as at 45 km depth about 7.09 ± 0.35 km/s (Figure 11b). Moreover, the low velocity gradients characterizing the whole crust below the MCP, with 0.05–0.06 km/s/km in the upper crust and 0.015 km/s/km for the rest of the crust, as the total thickness, are also in good agreement with continental crust.

Comparing the crustal structure with those of the surrounding areas of unquestionable continental nature from receiver functions studies, our values for the crustal thickness are of the same order of magnitude as that found for the undisturbed parts of the Zimbabwe and Kaapvaal Archean Cratons with a thickness of 35–40 km (Moulin et al., 2020). However, the crustal thickness in the MCP is lower than in the North part of the Kaapvaal Craton which has been disturbed by the Proterozoic event of the Bushveld Mafic Intrusion Complex (~2.05 Ga) and in the Archean inter-cratonic Limpopo Belt NW of the MCP (from 43 up to 50 km) (Delph & Porter, 2015; James et al., 2002; Nguuri et al., 2001; Nair et al., 2006; Youssef et al., 2013) (Figure 1b). Nevertheless, in term of velocities, the Kaapvaal Craton, at least in its undisturbed part, seems to present rather high velocities of 6.0–6.2 km/s for its upper part, whereas low velocities of 6.4–6.7 km/s are found in its lower part (Durrheim & Green, 1992). This observation strongly differs from our South of the MCP. Higher lower velocities (>7 km/s) are found for Proterozoic Terranes or parts of Archean Terranes affected by large-scale Proterozoic events due to mafic intrusions or underplating, but implying a much thicker crust (Durrheim & Mooney, 1991; Nguuri et al., 2001). The initial fabric of the MCP therefore remains uncertain compared with the deep structure of the surrounding areas. Its characteristics (significant crustal thickness, the velocity ranges and the low velocity gradients) nevertheless favor a continental nature of the crust, with probable modifications by magmatic materials responsible of velocities around 7 km/s in the lower part of the crust.

6.2. Nature of the Crust Below the NNV

The overall velocity architecture of the NNV appears clearly far from of the average velocity structure found for “normal” Atlantic-type Oceanic Crust of White et al., (1992), whether in term of thicknesses, velocities (>7.2 km/s) and velocity gradients. By contrast, the 1D velocity profiles profiles extracted along the MZ7 line have similar velocity trend to Continental crust (Figure 11b). In the CSS domain, the 1D velocity profiles show anyway a southward crustal thinning of about 10 km, that occurs mainly with a shallowing of the Moho limit. Looking further south, the 1D velocity profiles profiles from the S-NNV I to the South NNV-II exhibit the same trend as in the CSS with relatively low velocity gradients, a constant thickness and a flat Moho.

Further South, the C-NNV, the S-NNV II sub-domains correspond to areas of increasing velocities (with velocities > 7 km/s and up to 7.3–7.5 km/s at its base) compare to the two precedent sub-domains. High velocities in this range are known to occur in particular context, as for modified and intruded continental crust at some continental fragments, shields or rifts (Christensen & Mooney., 1995; Holbrook et al., 1992; Thybo et al., 2006, 2013), at transition of volcanic margins (Eldholm et al., 1995; Holbrook et al., 1993; Talwani et al., 2000), or at oceanic plateaus with thickened oceanic crust (e.g., North Kerguelen Plateau: Charvis et al., 1995; South Agulhas Plateau: Gohl & Uenzelmann-Neben et al., 2001; Ontong Java Plateau: Miura et al., 2004; South Mozambique Ridge: Gohl et al., 2011). Oceanic plateaus correspond to areas of anomalously thick oceanic crust formed by extensive basaltic magmatism, resulting in crustal thicknesses generally between 15 and 25 km, and of 21 ± 0.8 km in average (Ridley & Richards, 2010; Tetreault & Buitter, 2014). Only the 33 km-thick South Ontong Java Plateau (OJP) which appears as anomalously thick even for an oceanic plateau, as mentioned above, (Miura et al., 2004; Tetreault & Buitter, 2014) has a crustal thickness comparable with those if the NNV.

The final P-wave velocity structures obtained in the OJP (Miura et al., 2004) and in the NNV (this study) are both modeled using 4 crustal layers, the OJP including an about 15 km-thick bottom crustal layer with

P-wave velocities of 7.2–7.5 km/s. Nevertheless, disparities appear comparing the velocity architecture between the two regions: (1) The upper crustal top-bottom velocities in the range 4.8–5.6 km/s beneath the OJP, which are in the range of the oceanic Layer two (White et al., 1992), are not consistent with the upper crustal velocities in the NNV (5.6–6.8 km/s); (2) At the OJP, a velocity jump of 0.3 km/s from 6.8 to 7.2 km/s is present at the top of the deepest crustal layer whereas velocities increase more continuously from the middle crust to the lower crust in the NNV, and even through the whole crust; (3) The proportion of high-velocities in the range 7.2–7.5 km/s remains reduced in the NNV (<10 km) and more inhomogeneous laterally compared with the OJP. The same disparities emerge comparing the structure of the NNV with those of the South Agulhas Plateau and the South Mozambique ridge located directly S-SW of our study area, and considered as floored by over-thickened oceanic crust (Gohl et al., 2011; Gohl & Uenzelmann-Neben et al., 2001). In these both last cases, an half to two-thirds of the crustal column is characterized by velocities higher than 7 km/s, with increasing to 7.4–7.6 km/s at the base the crust. However, as at the OJP, P-wave velocity model shows lower upper crustal velocities (3.5–5.5 km/s MozR) and laterally homogeneous lower crustal velocities that differ with the NNV.

The continental break-up at volcanic passive margins is accompanied by significant volumes of melting, resulting in the intense production of extrusive flood-basalts indicated by characteristic Seaward Dipping Reflectors (SDRs) on normal-incidence seismic profiles, and high-velocity lower crust ($V_p > 7.2$ km/s) beneath the COB (e.g., Eldholm et al., 2000; Eldhom & Grue, 1994; Franke, 2013; Funck et al., 2017; Geoffroy et al., 2005; Guan et al., 2019). The nature of such high-velocities lower crust remains ambiguous since the exiting overlap between geophysical values and P-wave velocities, and the different possible corresponding lithologies. Early studies have proposed that the anomalous velocities represent mafic magmatic underplating (Furlong & Fountain, 1986; LASE Study Group, 1986) emplaced during initial stage of rifting and at least during the continental break-up, whereas more recent studies favor an heavily intruded continental crust by sills (Guan et al., 2019; White et al., 2008; White & Smith, 2009).

Setting aside the origin of these high velocities, the NNV remains thicker than the transitional domains at volcanic margins, which seems to rarely exceed 20 km thickness where high velocities are observed, while the important lateral extend of the high-velocity lower crust in the NNV is also unexpected, more than 400 km considering the whole N-S NNV (e.g., Bauer et al., 2000).

Last but not least, the 1D velocity depth profiles of the NNV is in perfect continuity with the velocity structure of the MCP (Figure 11), except for the thickness, implying a southwards step-by-step thinning of 10 km at the base of the continental crust. This evolution demonstrates the genetic link between the MCP and the NNV (Moulin et al., 2020).

Combined interpretation of the P-wave velocity modeling and reflection seismic reveals a first upper sedimentary sequence with velocities generally not exceeding 3 km/s, strongly thinning at the Central Terrace (less than 150 m) in the NNV. Distinct high velocity lenses associated with disturbed seismic facies on MZ7 MCS suggest the presence of inter-bedded volcanic sills, whilst in the Naude Ridge area clear post-sedimentary magmatism is imaged, attesting of the recurrence of magmatism episodes over time. The upper sedimentary sequence is underlain by a heterogeneous modeling sequence, labeled SV for sedimentary-volcanic sequence, characterized by intermediate velocities from 3.5 to 5.7 km/s. The younger sequence, especially in its upper portion SV1b, exhibits a large range of velocities, strong lateral velocity variations, as well as significant changes in seismic facies and reflector geometry on the MCS. This might notably reflect variations in the sediment/volcanic ratio, and furthermore raises the question of the continuity of the geological units especially South of the Central Terrace South of the NNV. We found major indications of deformation along the NNV: (a) tectonic activities or vertical movements through an alternation of southwards-dipping sub-basins and buried structural highs delimited by faults dipping toward the continent; (b) increasing indications of magmatism at the NR, the southernmost part of the NNV, in agreement with the strong positive peak (~600 nT) recorded in the magnetic field and the increasing modeled P-waves crustal velocities combined with the thinning of the crust below. The overprinting of the magmatic/tectonic episodes appear unsurprisingly important in the southern part of the NNV.

As proposed in Moulin et al., (2020), several magmatic events from Karoo (~183 Ma) to Miocene may have contributed to modify the crust in the NNV of continental nature, such as mafic intrusive bodies,

underplating or metamorphism, resulting in increasing of the P-waves velocities. The wide-angle data and the 1D velocity profiles analysis favor a continental nature of the whole area, which appears clearly disturbed by a succession of several magmatic events, responsible for intrusions and modifications of the crust. The C-NNV seems to localize a major magmatic intrusion around the location of the crossing with the MZ1 wide-angle profile (Figure 8). The disturbance appears to extend into the lower crust below the CSS, where high velocities up to 7.4–7.5 km/s are modeled at the base of the crust. This northern part is additionally marked by the occurrence of a smooth southward crustal thinning from the MCP toward the C-NNV.

The southernmost part of the NNV indicates clear evidence of crustal thinning in the NR area, as well as landward-dipping normal faults delineated several half grabens, morphological highs combined with southward dipping (i.e., seaward dipping) sub-basins and reflectors in the S-NNV II (Figures 4b and 10b). Although these seaward dipping reflectors imaged on the MCS data (Figure 4b), differ from the SDR wedge geometry (typically inner SDRs), as observed for example on the archetype conjugated volcanic margins of Argentina and South Africa (Franke, 2013). The succession of different magmatic events through time, and probably the associated readjustment by vertical movements have been superimposed in the South NNV. Furthermore, the NR area is clearly additionally overprinted by more recent post-sedimentary magmatism (~40 km model-distance, Figure 10b), increasing the complexity to correlate P-waves velocity anomalies to specific events as well as initial geometry of the necking zone. The present structure of the NNV is undoubtedly linked to volcanic activity, possibly pre- syn- post-breakup, and giving its present complex structure. The timing of the episodes and their importance remains to be defined and considered in the Natal Valley evolution.

The NR sub-domain corresponds to the real necking zone south of the NNV, with a decrease in crustal thickness from around 30–15 km, over a relatively sharp distance of 50 km. The chronology of the events is nevertheless difficult to determine with the MZ7 profile alone, due to the superimposition of events. Furthermore, the continuity of the upper sedimentary cover, as the SV sequence North and South of the Central Terrace is uncertain. Especially regarding the deep reflector included in the SV modeling sequence, which may deepen south of the Central Terrace (see from ~180 to 120 km model-distance, 3–4 stwt, Figure 10). In this sense, the series constituting the upper part of the volcano-sedimentary ensemble would then be more recent south of the Central Terrace. Additional higher resolution data would be required to resolve these uncertainties.

6.3. Localization of the Continent/Ocean Boundary

Velocity-depth profiles locate the necking zone in the southernmost part of the NNV, additionally revealing important evidences of magmatism, such as high crustal velocities (6.0–7.4 km/s), in the upper part of the crust compare to the North. The 1D velocity profiles extracted along the NR are situated between Continental and Oceanic Crust, and tend to become closer to the compilations for Oceanic crust moving southward (Figure 11c), mainly due to the decrease in crustal thickness combined with increasing velocity related to the different magmatic episodes. Directly South, the N-SNV presents a reduce crustal thickness around 10 km, and globally, a velocity-depth structure that seems more comparable with those of oceanic crust but this hypothesis is speculative due to the low constrains from the model given the low degree of coverage (and thus confidence) in that particular area (Figure 8).

Nevertheless, the presence of well-defined NW-SE aligned magnetic anomalies South to Tugela Ridge (Figure 1), connected with the movement of the Patagonia plate in Valanginian time, shows the presence of oceanic crust South of Tugela Ridge. Between the Tugela Ridge and the Naude ridge, any conclusion about the crustal nature is speculative without further information, but the presence of the abrupt necking zone of the Natal domain, the occurrence of the triple junction south Naude Ridge and the emplacement of the Dana & Galathea plateaux favor, the presence of transitional, oceanic or abnormal “proto-oceanic” crust (Afilhado et al., 2015; Klingelhoefer et al., 2015; Moulin et al., 2015) south of the MZ7 profile, at the edge between the clearly identifiable oceanic magnetic anomalies South of the S-TuR to the SE and the Mozambique Ridge to the East (Figure 1b).

We finally propose a position of the COB South of the NNV, South of the NR sub-domain probably at the location of the AG at the southernmost part of the MZ7 line. This position of the COB appears in relatively good agreement with the proposition of Goodlad (1986), revealing the important role of the ridges located at the junction between the North and South Natal Valley.

7. Conclusions

New data from the MZ7 deep seismic survey allowed to image continuously the crustal structure from the onshore MCP South Mozambique to the offshore N-SNV, passing through the whole North Natal Valley, and more local structures of the Naude Ridge and the Ariel Graben. This study presents insights about the N-S sedimentary and crustal architectures SE-Africa based on forward modeling of wide-angle seismic, coincident offshore MCS along with potential field data, in the context of Gondwana breakup and movement between the African-Antarctica-South American plates.

Our results favor a continental nature of the MCP as well as of the NNV. In the NNV, several intense magmatic activities have contributed to modify the propriety of the crust (e.g., $V_p > 7.2$ km/s). The C-NNV domain seems to localized a major magmatic intrusion including high velocities up to 7.5 km/s at the base of the crust, whereas the southernmost part of the NNV, at the NR, shows a general increase in velocities, on the whole crustal column, with no velocities lower than 6.0 km/s recorded through the crust and of 7.4 km/s at its base. From North to South, the ~ 35 –40 km thick crust gently thins under the South MCP and the CSS-NNV to about ~ 30 km in the major part of the NNV. The true, or major, necking zone is nevertheless located in the southernmost part of the NNV, in the area of the Naude Ridge, where the crust thins from ~ 30 km to around 10 km beneath the N-SNV, over a relatively sharp distance of about 50–60 km. Although less well constrained due to its position at the southernmost end of MZ7 the profile, the N-SNV does not seem to show such high velocities ($V_p > 7.2$ –7.3 km/s) at the base of the crust as modeled in the NNV. Its crustal thickness, as in general its velocity and seismic structures, appears more approximate to those of oceanic crust. These observations led us to interpret the N-SNV as atypical crust or proto-oceanic crust, and consequently to propose a location of the COB, close to the Ariel Graben location, South of the NR area and therefore at the junction between the NNV and the SNV.

Finally, the interpretation of the MCP as underlain by 40 km thick continental crust, of the NNV as underlain by intruded 30 km thick continental crust and the position of the necking zone preclude the possibility of an overlap of the Antarctica plate on the MCP and the NNV in Gondwana kinematic reconstructions (e.g., Leinweber & Jokat, 2012; Mueller & Jokat, 2019). This therefore favor models based on a looser fit as the recent model of Thompson et al. (2019), in which the place for continental crust in the MCP and NNV is allowed. The presence of well-defined NW-SE aligned magnetic anomalies South to Tugela Ridge which are connected with the movement of the Patagonia plate in Valanginian time seems to follow the inset of the thinning process of the necking zone of the NNV.

The age of the magmatic events, the direction of deformation and opening, as well as the probable link between both remain unclear with the MZ7 line alone. Further seismic data, with higher resolution, would help to solve the problem of the superimposition of the different phases, the precise orientation of the structures, particularly at the junction between the North and South Natal Valley, which underwent the movements between Africa-Antarctica (\sim N-S) and Africa-South America (\sim SW-NE), and the emplacement of the Mozambique Ridge. The precise nature and origin, formation of the N-SNV, between the S-TuR, E-Tur, NR is still enigmatic.

Data Availability Statement

The data of the PAMELA-MOZ3 (Moulin & Aslanian, 2016) and PAMELA-MOZ5 (Moulin & Evain, 2016) cruises are archived and referenced at SISMER and accessible on request at <https://doi.org/10.17600/16009500> and <https://doi.org/10.17600/16001600>

Acknowledgments

We thank the captain, crew, and MCS technical team of the R/V Pourquoi-Pas. We also thank the OBS technical team who maintain and constantly improve our OBS pool, as well as the land stations deployment team. We thank the Editor, Michael Bostock, the associated editor, the reviewer Laura Gómez de la Peña and one other anonymous reviewer for their comments, which substantially improved the manuscript. The PAMELA (Passive Margins Exploration Laboratories) project was initiated in the early 2010th by TOTAL and IFREMER in collaboration with French universities (Université de Bretagne Occidentale, Université Rennes 1, Université Pierre and Marie Curie), the CNRS and the IFPEN. A Leprêtre and F. Verrier respective post-doc studies and contract were co-funded by TOTAL and Ifremer as part of the PAMELA (Passive Margin Exploration Laboratories) scientific project. The GMT (Wessel & Smith, 1998), Seismic Unix (Cohen & Stockwell, 2003; Stockwell, 1999), and Geocluster (CGG-Veritas) software packages were used extensively in this study.

References

Afilhado, A., Moulin, M., Aslanian, D., Schnürle, P., Klingelhoefer, F., Rabineau, M., et al. (2015). Deep crustal structure across an young passive margin from wide-angle and reflection seismic data (The Sardinia Experiment) - II: Sardinia's margin. *Bulletin de la Société Géologique de France*, 186(4–5), 331–351. <https://doi.org/10.2113/gssgfbull.186.4-5.331>

Auffret, K., Pelleau, P., Klingelhoefer, F., Geli, L., Crozon, J., Lin, J.-Y., et al. (2004). MicroOBS: A new generation of ocean bottom seismometer. *First Break*, 22(7), 41–47. <https://doi.org/10.3997/1365-2397.2004012>

Bauer, K., Neben, S., Schreckenberger, B., Emmermann, R., Hinz, K., Fechner, N., et al. (2000). Deep structure of the Namibia continental margin as derived from integrated geophysical studies. *Journal of Geophysical Research*, 105, 25829–25853. <https://doi.org/10.1029/2000jb900227>

Charvis, P., & Operto, S. (1999). Structure of the Cretaceous Kerguelen Volcanic Province (southern Indian Ocean) from wide-angle seismic data. *Journal of Geodynamics*, 28, 51–71. [https://doi.org/10.1016/S0264-3707\(98\)00029-5](https://doi.org/10.1016/S0264-3707(98)00029-5)

Charvis, P., Recq, M., Operto, S., & BREFORT, D. (1995). Deep structure of the northern Kerguelen Plateau and hotspot-related activity. *Geophysical Journal International*, 122, 899–924. <https://doi.org/10.1111/j.1365-246x.1995.tb06845.x>

Christensen, N. I., & Mooney, W. D. (1995). Seismic velocity structure and composition of the continental crust: A global view. *Journal of Geophysical Research*, 100, 9761. <https://doi.org/10.1029/95jb00259>

Christeson, G. L., Goff, J. A., & Reece, R. S. (2019). Synthesis of oceanic crustal structure from two-dimensional seismic profiles. *Reviews of Geophysics*, 57, 504–529. <https://doi.org/10.1029/2019rg000641>

Cohen, J. K., & Stockwell, J. W., Jr (2003). *CWP/SU: Seismic Unix release 37: An open source package for seismic research and processing*. Center for Wave Phenomena, Colorado School of Mines.

Cox, K. G. (1992). Karoo igneous activity, and the early stages of the break-up of Gondwanaland. In B. C. Storey, T. Alabaster, & R. J. Pankhurst, Eds., *Magmatism and the causes of continental break-up* Vol. (68, pp. 137–148). Geol. Soc. London Spec. Publ.

Darracott, B. W. (1974). On the crustal structure and evolution of southeastern Africa and the adjacent Indian Ocean. *Earth and Planetary Science Letters*, 24(2), 282–290. [https://doi.org/10.1016/0012-821x\(74\)90106-x](https://doi.org/10.1016/0012-821x(74)90106-x)

Delph, J. R., & Porter, R. C. (2015). Crustal structure beneath southern Africa: Insight into how tectonic events affect the Mohorovicic discontinuity. *Geophysical Journal International*, 200, 254–264.

Dingle, R. V., & Scrutton, R. A. (1974). Continental breakup and the development of post-Paleozoic sedimentary basins around southern Africa. *The Geological Society of America Bulletin*, 85, 1467–1474. [https://doi.org/10.1130/0016-7606\(1974\)85<1467:cbatdo>2.0.co;2](https://doi.org/10.1130/0016-7606(1974)85<1467:cbatdo>2.0.co;2)

Domingues, A., Silveira, G., Ferreira, A. M. G., Chang, S.-J., Custódio, S., & Fonseca, J. F. B. D. (2016). Ambient noise tomography of the East African Rift in Mozambique. *Geophysical Journal International*, 204, 1565–1578. <https://doi.org/10.1093/gji/ggv538>

Durrheim, R. J., & Green, R. W. E. (1992). A seismic refraction investigation of the Archean Kaapvaal Craton, South Africa, using mine tremors as the energy source. *Geophysical Journal International*, 108, 812–832. <https://doi.org/10.1111/j.1365-246x.1992.tb03472.x>

Durrheim, R. J., & Mooney, W. D. (1991). Archean and Proterozoic crustal evolution: Evidence from crustal seismology. *Geol*, 19(6), 606–609. [https://doi.org/10.1130/0091-7613\(1991\)019<0606:aapcee>2.3.co;2](https://doi.org/10.1130/0091-7613(1991)019<0606:aapcee>2.3.co;2)

Eldholm, O., Gladchenko, T. P., Skogseid, J., & Planke, S. (2000). Atlantic volcanic margins: A comparative study. *Geological Society, London, Special Publications*, 167, 411–428. <https://doi.org/10.1144/gsl.sp.2000.167.01.16>

Eldholm, O., Skogseid, J., Planke, S., & Gladchenko, T. P. (1995). Volcanic Margin Concepts. In E. Banda, M. Torné, & M. Talwani, Eds., *Rifted ocean-continent boundaries*. NATO ASI series (series C: Mathematical and physical sciences) Vol. (463). Dordrecht: Springer.

Eldholm, O., & Grue, K. (1994). North Atlantic volcanic margins: Dimensions and production rates. *Journal of Geophysical Research*, 99(B2), 2955–2968.

Franke, D. (2013). Rifting, lithosphere breakup and volcanism: Comparison of magma-poor and volcanic rifted margins. *Marine and Petroleum Geology*, 43, 63–87. <https://doi.org/10.1016/j.marpetgeo.2012.11.003>

Funck, T., Erlendsson, Ö., Geissler, W. H., Gradmann, S., Kimbell, G. S., McDermott, K., et al. (2017). A review of the NE Atlantic conjugate margins based on seismic refraction data. *Geological Society, London, Special Publications*, 447, 171–205. <https://doi.org/10.1144/sp447.9>

Furlong, K. P., & Fountain, D. M. (1986). Continental crustal underplating: Thermal considerations and seismic-petrologic consequences. *Journal of Geophysical Research*, 91(B8), 8285–8294. <https://doi.org/10.1029/jb091ib08p08285>

Geoffroy, L. (2005). Volcanic passive margins. *Comptes Rendus Geoscience*, 337, 1395–1408. <https://doi.org/10.1016/j.crte.2005.10.006>

Gohl, K., & Uenzelmann-Neben, G. (2001). The crustal role of the Agulhas Plateau, southwest Indian Ocean: evidence from seismic profiling. *Geophysical Journal International*, 144, 632–646. <https://doi.org/10.1046/j.1365-246x.2001.01368.x>

Gohl, K., Uenzelmann-Neben, G., & Grobys, N. (2011). Growth and dispersal of a southeast African large igneous province. *South African Journal of Geology*, 114(3–4), 379–386. <https://doi.org/10.2113/gssajg.114.3-4.379>

Goodlad, S. W. (1986). Tectonic and sedimentary history of the Mid-Natal Valley (S.W. Indian Ocean). *Joint Geol/University of Cape Town Mar. Geosci. Unit Bull.*, 15, 1–415.

Goodlad, S. W., Martin, A. K., & Hartnady, C. J. H. (1982). Mesozoic magnetic anomalies in the southern Natal Valley. *Nature*, 295, 686–688. <https://doi.org/10.1038/295686a0>

Green, A. G. (1972). Seafloor spreading in the Mozambique Channel. *Nature Physical Science*, 236, 19–21. <https://doi.org/10.1038/physci236019a0>

Grevemeyer, I., Ranero, C. R., & Ivandic, M. (2018). Structure of oceanic crust and serpentinization at subduction trenches. *Geosphere*, 14(2), 395–418. <https://doi.org/10.1130/ges01537.1>

Guan, H., Geoffroy, L., Gernigon, L., Chauvet, F., Grigné, C., & Werner, P. (2019). Magmatic ocean-continent transitions. *Marine and Petroleum Geology*, 104, 438. <https://doi.org/10.1016/j.marpetgeo.2019.04.003>

Hanyu, T., Nogi, Y., & Fujii, M. (2017). Crustal formation and evolution processes in the Natal Valley and Mozambique Ridge, off South Africa. *Polar Science*, 13, 66–81. <https://doi.org/10.1016/j.polar.2017.06.002>

Holbrook, W. S., & Kelemen, P. B. (1993). Large igneous province on the US Atlantic margin and implications for magmatism during continental breakup. *Nature*, 364, 433–436. <https://doi.org/10.1038/364433a0>

Holbrook, W. S., Mooney, W. D., & Christensen, N. I. (1992). The seismic velocity structure of the deep continental crust. In D. M. Fountain, R. Arculus, & R. Kay, Eds., *Lower continental crust* (pp. 1–43). Amsterdam: Elsevier.

James, D. E., & Fouch, M. J. (2002). Formation and evolution of Archean cratons: Insights from southern Africa. *Geological Society, London, Special Publications*, 199, 1–26. <https://doi.org/10.1144/gsl.sp.2002.199.01.01>

Jourdan, F., Féraud, G., Bertrand, H., Watkeys, M. K., & Renne, P. R. (2008). The ⁴⁰Ar/³⁹Ar ages of the sill complex of the Karoo large igneous province: Implications for the Pliensbachian-Toarcian climate change. *Geochemistry, Geophysics, Geosystems*, 9, Q06009. <https://doi.org/10.1029/2008gc001994>

- Klausen, M. B. (2009). The Lebombo monocline and associated feeder dyke swarm: Diagnostic of a successful and highly volcanic rifted margin? *Tectonophysics*, *468*, 42–62. <https://doi.org/10.1016/j.tecto.2008.10.012>
- Klingelhoefer, F., Evain, M., Afilhado, A., Rigoti, C., Loureiro, A., Alves, D., et al. (2015). Imaging proto-oceanic crust off the Brazilian Continental Margin. *Geophysical Journal International*, *200*(1), 471–488. <https://doi.org/10.1093/gji/ggu387>
- König, M., & Jokat, J. (2010). Advanced insights into magmatism and volcanism of the Mozambique Ridge and Mozambique Basin in the view of new potential field data. *Geophysical Journal International*, *180*, 158–180. <https://doi.org/10.1111/j.1365-246X.2009.04433.x>
- LASE Study Group. (1986). Deep structure of the US East Coast passive margin from large aperture seismic experiments (LASE). *Marine and Petroleum Geology*, *3*(3), 234–240.
- Leinweber, V., & Jokat, W. (2011). Is there continental crust underneath the northern Natal Valley and the Mozambique Coastal Plains? *Geophysical Research Letters*, *38*, 87–101. <https://doi.org/10.1029/2011gl047659>
- Leinweber, V. T., & Jokat, W. (2012). The Jurassic history of the Africa-Antarctica corridor - new constraints from magnetic data on the conjugate continental margins. *Tectonophysics*, *530–531*, 87–101. <https://doi.org/10.1016/j.tecto.2011.11.008>
- Loureiro, A., Afilhado, A., Matias, L., Moulin, M., & Aslanian, D. (2016). Monte Carlo approach to assess the uncertainty of wide-angle layered models: Application to the Santos Basin, Brazil. *Tectonophysics*, *683*, 286–307. <https://doi.org/10.1016/j.tecto.2016.05.040>
- Lutter, W. J., & Nowack, R. L. (1990). Inversion for crustal structure using reflections from the PASSCAL Ouachita Experiment. *Journal of Geophysical Research*, *95*, 4633–4646. <https://doi.org/10.1029/jb095ib04p04633>
- Martin, A. K., & Hartnady, C. J. H. (1986). Plate tectonic development of the south west Indian Ocean: A revised reconstruction of East Antarctica and Africa. *Journal of Geophysical Research*, *91*(B5), 4767–4786. <https://doi.org/10.1029/jb091ib05p04767>
- Miura, S., Suyehiro, K., Shinohara, M., Takahashi, N., Araki, E., & Taira, A. (2004). Seismological structure and implications of collision between the Ontong Java Plateau and Solomon Island Arc from ocean bottom seismometer-airgun data. *Tectonophysics*, *389*, 191–220. <https://doi.org/10.1016/j.tecto.2003.09.029>
- Moulin, M., & Aslanian, D. (2016). PAMELA-MOZ03 cruise, RV *Pourquoi pas?* <http://doi.org/10.17600/16001600>
- Moulin, M., Aslanian, D., Evain, M., Leprêtre, A., Schnurle, P., Verrier, F., et al., & the PAMELA-MOZ35 team. (2020). Gondwana breakup: Messages from the North Natal Valley. *Terra Nova*, *32*, 205–214. <https://doi.org/10.1111/ter.12448>
- Moulin, M., Aslanian, D., & Unternehr, P. (2010). A new starting point for the south and equatorial Atlantic Ocean. *Earth-science Reviews*, *98*, 1–37. <https://doi.org/10.1016/J.Earscirev.2009.08.001>
- Moulin, M., & Evain, M. (2016). PAMELA-MOZ05 cruise, RV *Pourquoi pas?* <http://doi.org/10.17600/16009500>
- Moulin, M., Klingelhoefer, F., Afilhado, A., Aslanian, D., Schnurle, P., Nouzé, H., et al. (2015). Deep crustal structure across an young passive margin from wide-angle and reflection seismic data (The Sardinia Experiment) - I. Gulf Of Lion's margin. *Bulletin de la Société Géologique de France*, *186*(4–5), 309–330. <https://doi.org/10.2113/gssgfbull.186.4-5.309>
- Mueller, C.O., & Jokat, W. (2017). Geophysical evidence for the crustal variation and distribution of magmatism along the central coast of Mozambique. *Tectonophysics*, *712–713*, 684–703. <https://doi.org/10.1016/j.tecto.2017.06.007>
- Mueller, C. O., & Jokat, W. (2019). The initial Gondwana break-up: A synthesis based on new potential field data of the Africa-Antarctica Corridor. *Tectonophysics*, *750*, 301–328. <https://doi.org/10.1016/j.tecto.2018.11.008>
- Nair, S. K., Gao, S. S., Liu, K. H., & Silver, P. G. (2006). Southern African crustal evolution and composition: Constraints from receiver function studies. *Journal of Geophysical Research: Solid Earth*, *111*, B02304. <https://doi.org/10.1029/2005jb003802>
- Nguuri, T. K., Gore, J., James, D. E., Webb, S. J., Wright, C., Zengeni, T. G., et al. (2001). Crustal structure beneath southern Africa and its implications for the formation and evolution of the Kaapvaal and Zimbabwe cratons. *Geophysical Research Letters*, *28*(13), 2501–2504. <https://doi.org/10.1029/2000gl012587>
- Nguyen, L. C., Hall, S. A., Bird, D. E., & Ball, P. J. (2016). Reconstruction of the East Africa and Antarctica continental margins. *Journal of Geophysical Research: Solid Earth*, *121*, 4156–4179. <https://doi.org/10.1002/2015JB012776>
- Patriat, M., Klingelhoefer, F., Aslanian, D., Contrucci, C., Gutscher, M.-A., Talandier, J., et al. (2002). Deep crustal structure of the Tuamotu plateau and Tahiti (French Polynesia) based on seismic refraction data. *Geophysical Research Letters*, *29*, 1–4. <https://doi.org/10.1029/2001GL013913>
- Reeves, C., Teasdale, J. P., & Mahanjane, E. S. (2016). Insight into the Eastern Margin of Africa from a new tectonic model of the Indian Ocean. In M. Nemcok, S. Rybar, S. T. Sinha, S. A. Hermeston, & L. Ledvényiova, Eds., *Transform margins; development, controls and petroleum systems*. Geol. Soc. Lond. Vol. (431). Spec. Publ. <http://doi.org/10.1144/SP431.12>
- Ridley, V. A., & Richards, M. A. (2010). Deep crustal structure beneath large igneous provinces and the petrologic evolution of flood basalts. *Geochemistry, Geophysics, Geosystems*, *11*, Q09006. <https://doi.org/10.1029/2009gc002935>
- Ryan, W. B. F., Carbotte, S. M., Coplan, J. O., O'Hara, S., Melkonian, A., Arko, R., et al. (2009). Global Multi-Resolution Topography synthesis. *Geochemistry, Geophysics, Geosystems*, *10*, Q03014. <https://doi.org/10.1029/2008GC002332>
- Sandwell, D. T., & Smith, W. H. F. (2009). Global marine gravity from retracked Geosat and ERS-1 altimetry: Ridge segmentation versus spreading rate. *Journal of Geophysical Research*, *114*, B01411. <https://doi.org/10.1029/2008JB006008>
- Schneider, W. A., & Backus, M. M. (1964). Ocean-bottom seismic measurements off the California coast. *Journal of Geophysical Research*, *69*(6), 1135–1143. <https://doi.org/10.1029/jz069i006p01135>
- Stockwell, J. W., Jr (1999). The CWP/SU: Seismic Un*x package. *Computers & Geosciences*, *25*(4), 415–419. [https://doi.org/10.1016/S0098-3004\(98\)00145-9](https://doi.org/10.1016/S0098-3004(98)00145-9)
- Talwani, M., & Abreu, V. (2000). Inferences regarding initiation of oceanic crust formation from the U.S. East Coast margin and conjugate South Atlantic margins. In W. U. Mohriak, & M. Talwani, Eds., *Atlantic rifts and continental margins* (115 (pp. 211–233)). AGU Geophysical Monograph.
- Tetreault, J. L., & Buter, S. J. H. (2014). Future accreted terranes: A compilation of island arcs, oceanic plateaus, submarine ridges, sea-mounts, and continental fragments. *Solid Earth*, *5*, 1243–1275. <https://doi.org/10.5194/se-5-1243-2014>
- Thompson, J. O., Moulin, M., Aslanian, D., de Clarens, P., & Guilloucheau, F. (2019). New starting point for the Indian Ocean: Second phase of breakup for Gondwana. *Earth-Science Reviews*, *191*, 26–56. <https://doi.org/10.1016/j.earscirev.2019.01.018>
- Thybo, H., & Artemieva, I. M. (2013). Moho and magmatic underplating in continental lithosphere. *Tectonophysics*, *609*, 605–619. <https://doi.org/10.1016/j.tecto.2013.05.032>
- Thybo, H., Sandrin, A., Nielsen, L., Lykke-Andersen, H., & Keller, G. R. (2006). Seismic velocity structure of a large mafic intrusion in the crust of central Denmark from project ESTRID. *Tectonophysics*, *420*, 105–122. <https://doi.org/10.1016/j.tecto.2006.01.029>
- Tikku, A. A., Marks, K. M., & Kovacs, L. C. (2002). An early cretaceous extinct spreading center in the northern Natal valley. *Tectonophysics*, *347*, 87–108. [https://doi.org/10.1016/s0040-1951\(01\)00239-6](https://doi.org/10.1016/s0040-1951(01)00239-6)
- Wessel, P., & Smith, W. H. F. (1998). *New, improved version of generic mapping tools released*, (p. 579). EOS. AGU.

- White, R. S., McKenzie, D., & O'Nions, R. K. (1992). Oceanic crustal thickness from seismic measurements and rare earth element inversions. *Journal of Geophysical Research*, 97(B13), 19683–19715. <https://doi.org/10.1029/92jb01749>
- White, R. S., & Smith, L. K. (2009). Crustal structure of the Hatton and the conjugate East Greenland rifted volcanic continental margins, NE Atlantic. *Journal of Geophysical Research*, 114, B02305. <https://doi.org/10.1029/2008jb005856>
- White, R. S., Smith, L. K., Smith, L. K., Roberts, A. W., Christie, P. A. F., & Kuszniir, N. J., & the rest of the iSIMM Team. (2008). Lower-crustal intrusion on the North Atlantic continental margin. *Nature*, 452, 460–464. <https://doi.org/10.1038/nature06687>
- Youssof, M., Thybo, H., Artemieva, I. M., & Levander, A. (2013). Moho depth and crustal composition in southern Africa. *Tectonophysics*, 609, 267–287. <https://doi.org/10.1016/j.tecto.2013.09.001>
- Zelt, C. A. (1999). Modeling strategies and model assessment for wide-angle seismic traveltimes. *Geophysical Journal International*, 139, 183–204. <https://doi.org/10.1046/j.1365-246x.1999.00934.x>
- Zelt, C. A., & Forsyth, D. A. (1994). Modeling wide-angle seismic data for crustal structure: Southeastern Grenville province. *Journal of Geophysical Research*, 99, 11687–11704. <https://doi.org/10.1029/93JB02764>
- Zelt, C. A., & Smith, R. B. (1992). Seismic traveltimes inversion for 2-D crustal velocity structure. *Geophysical Journal International*, 108, 16–34. <https://doi.org/10.1111/j.1365-246x.1992.tb00836.x>